Chemical Geology 268 (2009) 298–312

Contents lists available at ScienceDirect

Chemical Geology

journal homepage: www.elsevier.com/locate/chemgeo

Geochemical investigation of Early Cretaceous igneous rocks along an east–west traverse throughout the central Lhasa Terrane, Tibet

Di-Cheng Zhu [a,b,*], Xuan-Xue Mo [a,b], Yaoling Niu [c], Zhi-Dan Zhao [a,b], Li-Quan Wang [d], Yong-Sheng Liu [e], Fu-Yuan Wu [f]

[a] State Key Laboratory of Geological Processes and Mineral Resources, China University of Geosciences, Beijing 100083, China
[b] School of Earth Science and Resources, China University of Geosciences, Beijing 100083, China
[c] Department of Earth Sciences, Durham University, Durham DH1 3LE, UK
[d] Chengdu Institute of Geology and Mineral Resources, Chengdu 610082, China
[e] State Key Laboratory of Geological Processes and Mineral Resources, China University of Geosciences, Wuhan 430074, China
[f] Institute of Geology and Geophysics, Chinese Academy of Sciences, Beijing 100029, China

ARTICLE INFO

Article history:
Received 19 February 2009
Received in revised form 5 September 2009
Accepted 8 September 2009

Editor: R.L. Rudnick

Keywords:
Bulk-rock geochemistry
Zircon U–Pb dating and Hf isotope
Petrogenesis
Early Cretaceous igneous rocks
Slab break-off
Bangong–Nujiang Tethyan Ocean
Tectonomagmatic evolution
Lhasa micro-continental block
Tibet

ABSTRACT

Bulk-rock major and trace element, Sr–Nd isotope, zircon U–Pb and Hf-isotope data are reported for Early Cretaceous igneous rocks sampled along an east–west traverse through the central Lhasa subterrane (E80°00′–E89°) in southern Tibet. These results offer new insights into the pre-Cenozoic geology and tectonomagmatic evolution of the Lhasa Terrane, and provide boundary conditions for the origin and evolution of the Tibetan Plateau. Our new data, together with data from the literature indicate that the Early Cretaceous magmatism in the central Lhasa subterrane lasted for a long period (~143–102 Ma) with a magmatic flare-up at ~110 Ma. The latter is accompanied by mafic magmatism in this terrane. The silicic rocks are metaluminous to peraluminous, and enriched in Rb, Th, and U, and depleted in Ba, Nb, Ta, Sr, P, and Ti, with varying initial $^{87}Sr/^{86}Sr$ (0.7073–0.7209), negative $\varepsilon_{Nd}(t)$ (−13.7 to −4.6), and negative to positive zircon $\varepsilon_{Hf}(t)$. The andesitic and dioritic enclaves are characterized by initial $^{87}Sr/^{86}Sr$ of 0.7088–0.7148, $\varepsilon_{Nd}(t)$ of −9.9 to −7.8, and zircon $\varepsilon_{Hf}(t)$ of −9.5 to −0.2, similar to those of the 110±3 Ma silicic rocks. The bulk-rock Sr and Nd isotopic data and zircon $\varepsilon_{Hf}(t)$ values indicate an increased contribution of a mantle component in the generation of the Early Cretaceous igneous rocks in the central Lhasa subterrane at ~110 Ma. Available bulk-rock Nd- and zircon Hf-isotope data indicate that the crust of the central Lhasa subterrane, at least its oldest elements, was emplaced during the Archean. This further indicates that the central Lhasa subterrane with ancient basement must have been a micro-continental block (i.e., the Lhasa micro-continental block) extending in an east–west direction for >700 km (E82°–E89°) with a width of ~100 km. The contemporaneous presence of S-type (more crustal source) and I-type (significant mantle input) melts of the Early Cretaceous igneous rocks in this subterrane are interpreted as the consequences of varying extents of interactions between the existing continental crust and mantle-derived melts (including crustal anatexis). We suggest that the mantle-derived melts resulted from southward subduction of the Bangong–Nujiang Ocean seafloor in a syncollisional setting related to the Lhasa–Qiangtang collision, and that the magmatic flare-up with strong mantle input at ~110 Ma was genetically associated with the slab break-off of this subducting seafloor.

1. Introduction

The Lhasa Terrane in southern Tibet (Fig. 1a) has long been accepted as a tectonic block rifted from Gondwana and drifted northward across the Tethyan oceans (see Dewey et al., 1988; Yin and Harrison, 2000, and references therein). Its collision with the Qiangtang Terrane to the north marked the closure of the Paleo-Tethyan (or Bangong–Nujiang) Ocean in the early Cretaceous (Dewey et al., 1988; Yin and Harrison, 2000; Zhang et al., 2004; Kapp et al., 2005a, 2007; Leier et al., 2007a,b), and its subsequent collision with the northward moving Indian continent marked the closure of the Neo-Tethyan Ocean in the early Cenozoic (see Mo et al., 2003, 2007, 2008; Chung et al., 2005). While this conceptual framework is straightforward, its validity needs testing and geological processes involved in time and space need understanding. The Mesozoic magmatic rocks in the Lhasa Terrane as a result of these processes must record these processes and therefore afford opportunities to understand the evolution of the Tethyan Ocean basins and boundary conditions for models of the origin and evolution of the Tibetan Plateau.

* Corresponding author. State Key Laboratory of Geological Processes and Mineral Resources, China University of Geosciences, 29# Xue-Yuan Road, Haidian District, Beijing 100083, China. Tel./fax: +86 10 8232 2094.
E-mail address: dchengzhu@163.com (D.-C. Zhu).

0009-2541/$ – see front matter © 2009 Elsevier B.V. All rights reserved.
doi:10.1016/j.chemgeo.2009.09.008

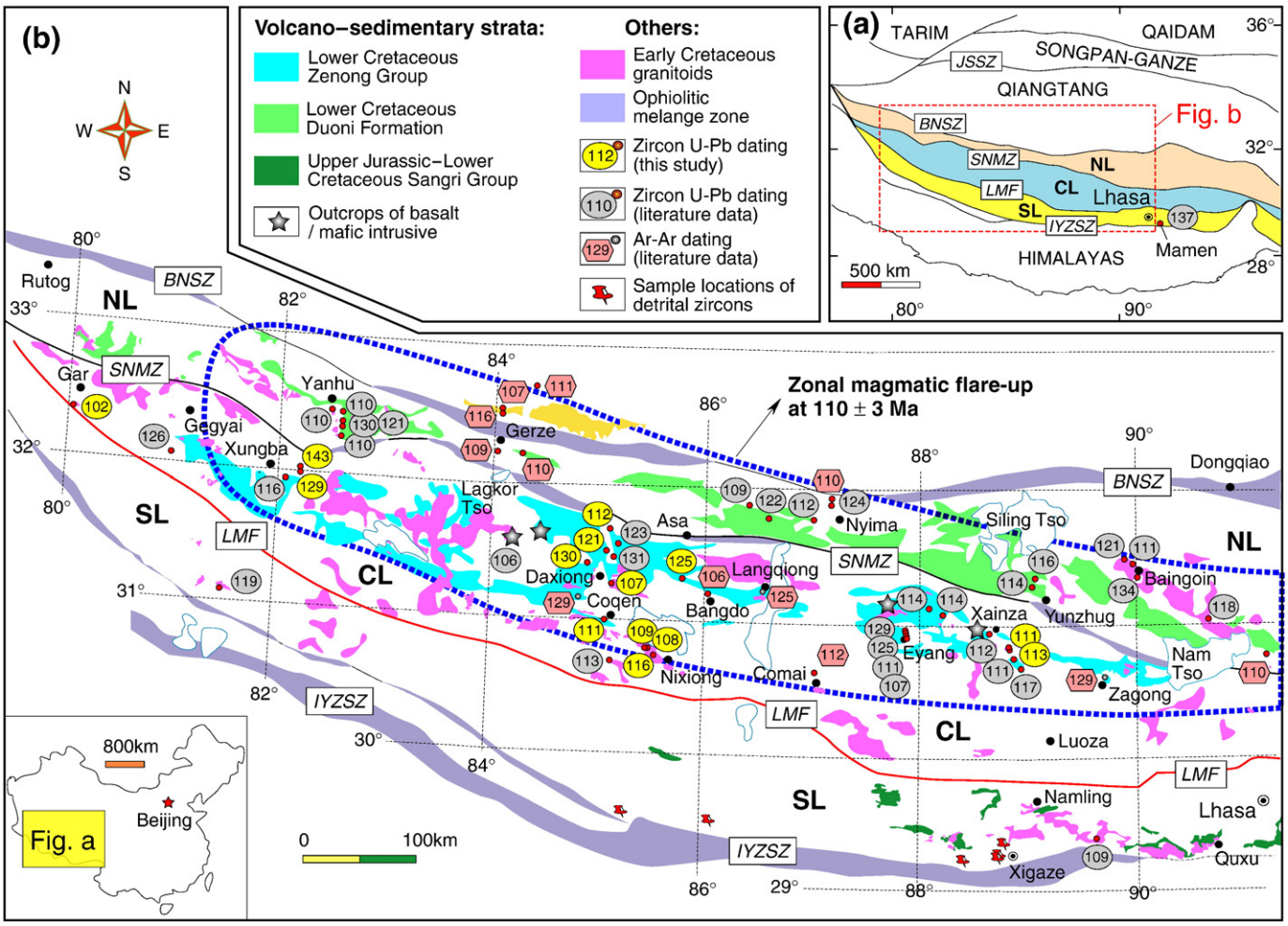

Fig. 1. (a) Tectonic outline of the Tibetan Plateau showing the study area (Zhu et al., 2008a). JSSZ = Jinsha Suture Zone; BNSZ = Bangong–Nujiang Suture Zone; SNMZ = Shiquanhe–Nam Tso Mélange Zone; LMF = Luobadui–Milashan Fault; IYZSZ = Indus–Yarlung Zangbo Suture Zone. NL = Northern Lhasa subterrane; CL = Central Lhasa subterrane; SL = Southern Lhasa subterrane. (b) Tectonic framework of the Lhasa Terrane showing major tectonic subdivisions, distribution of Early Cretaceous igneous rocks (Zhang et al., 2004; Zhu et al., 2008b), and localities of dated igneous rocks (ovals with numerals). Literature data include Liu et al. (2003), Schwab et al. (2004), Kapp et al. (2005a, 2007), Leier et al. (2007a), Volkmer et al. (2007), Zhu et al. (2008c, 2009a, submitted for publication, unpublished data), Lee et al. (2009), and Ji et al. (2009a).

Some relevant data on the Mesozoic geology of the Lhasa Terrane exist, but they are inadequate and their interpretations are mostly questionable. For example, it is known that Early Cretaceous igneous rocks are widespread throughout the northern parts of the Lhasa Terrane (north of the Gangdese batholiths) (Fig. 1b), but how the magmatism may have evolved in time and space in terms of magma source materials and mechanism of magma generation remains poorly known because the existing data neither have adequate spatial coverage nor have needed space–time resolution. As a result, existing interpretations on the petrogenesis and tectonomagmatic processes during the Early Cretaceous are speculative and conflicting. These rocks have been considered to be a bimodal suite consisting of (a) peraluminous two-mica granites derived from crustal anatexis and (b) biotite-hornblende granodiorites as a result of mantle-derived melts with significant crustal assimilation overlaying a seafloor lithosphere that continued to subduct or underthrust after the collision (Xu et al., 1985; Harris et al., 1988a,b, 1990; Pearce and Mei, 1988) or generated by a low-angle northward subduction of the Neo-Tethyan Ocean seafloor (Coulon et al., 1986). Recent studies on the Mesozoic igneous rocks sampled along a north–south traverse from Xigaze, via Namling, Luoza, and Xainza, to Siling Tso/Nyima across the Lhasa Terrane (Fig. 1b) argue that these igneous rocks may have been associated in time and space with the southward subduction of the Bangong–Nujiang Ocean seafloor beneath the Lhasa Terrane (Zhu et al., submitted for publication).

As part of a systematic study of the pre-Cenozoic magmatism in the northern part of the Lhasa Terrane (north of the Gangdese batholiths), we report here a dataset on bulk-rock major and trace element compositions, Sr–Nd isotope analyses, zircon U–Pb ages on 10 samples and zircon Hf isotopic analyses on 13 samples of Early Cretaceous igneous rocks. These include andesite, dacite, rhyolite, rhyolitic tuff, dioritic enclaves and host granodiorite along an east–west traverse throughout the central Lhasa Terrane (E80°00′–E89°′) (Fig. 1b) in southern Tibet. These new data, in combination with data in the recent literature (Zhou et al., 2008; Ji et al., 2009a; Zhu et al., submitted for publication; Zhao et al., in press), are used to illustrate (1) the lithospheric architecture of the Lhasa Terrane, (2) the mechanism of magma generation during the Early Cretaceous, and (3) the evolution of the Tethyan Ocean basins in the Early Cretaceous. These results offer new perspectives on crustal growth (Mo et al., 2008) in general and insights into the tectonomagmatic evolution in southern Tibet before the India–Asia collision in particular.

2. Geological background

Geologically, the Tibetan Plateau (the southern portion of the Qinghai–Tibetan Plateau) comprises, from north to south, the following four blocks or terranes: the Songpan–Ganzi flysch complex, Qiangtang Terrane, Lhasa Terrane and the Himalaya. These blocks are separated by

the Jinsha (JSSZ), Bangong–Nujiang (BNSZ), and Indus–Yarlung Zangbo (IYZSZ) suture zones, representing Paleo-, Meso-, and Neo-Tethyan oceanic relics, respectively (Fig. 1a) (see Yin and Harrison, 2000).

The Lhasa Terrane, which is bounded to the north by the BNSZ and to the south by the IYZSZ (Fig. 1a), can be divided into northern, central, and southern subterranes, separated by the Shiquanhe–Nam Tso Mélange Zone (SNMZ) and Luobadui–Milashan Fault (LMF), respectively (Fig. 1b). The northern Lhasa subterrane is inferred to be underlain by a Cambrian or Neoproterozoic crystalline basement, which was reported only from the Amdo area (Amdo orthogneiss) (Xu et al., 1985; Dewey et al., 1988; Guynn et al., 2006). The main rock units exposed in this subterrane are Jurassic–Cretaceous sedimentary and associated igneous rocks (Leeder et al., 1988; Yin et al., 1988; Pan and Ding, 2004; Zhang et al., 2004; Leier et al., 2007a,b; Zhu et al., 2008a). The central Lhasa subterrane consists mostly of a Carboniferous–Permian metasedimentary sequence, a Lower Cretaceous volcano-sedimentary sequence (e.g., Zenong Group) and associated granitoids with minor Ordovician, Silurian, and Triassic limestones (Leeder et al., 1988; Yin et al., 1988; Pan and Ding, 2004; Kapp et al., 2005a; Ji et al., 2007; Leier et al., 2007a,b; Zhu et al., 2008a) and rare Precambrian strata (Hu et al., 2005). The southern Lhasa subterrane is dominated by the Cretaceous to early Tertiary Gangdese batholiths and Linzizong volcanic succession with minor Triassic–Cretaceous volcano-sedimentary rocks (Leeder et al., 1988; Pearce and Mei, 1988; Pan and Ding, 2004; Chung et al., 2005; He et al., 2007; Leier et al., 2007a; Mo et al., 2007, 2008; Wen et al., 2008; Zhu et al., 2008a, 2009a).

Conventionally, the Lhasa Terrane is considered not only as an archetype of a Cenozoic orogen as a result of India–Asia continental collision, but also as an Andean-type active continental margin genetically associated with the northward subduction of the Neo-Tethyan seafloor prior to the India–Asia collision marked by the IYZSZ (Maluski et al., 1982; Xu et al., 1985; Coulon et al., 1986; XBGMR, 1991; Copeland et al., 1995; Chung et al., 2005; Chu et al., 2006; Wen et al., 2008; Zhu et al., 2008a,b, 2009a). Recently, the recognition of polarity variation of $\varepsilon_{Hf}(t)$ values of zircons separated from the Mesozoic silicic rocks from a N–S transect of Xigaze–Namling–Luoza–Xainza–Nyima/Siling Tso across the Lhasa Terrane (Fig. 1b) led Zhu et al. (submitted for publication) to suggest that much of the Mesozoic magmatism is associated with the southward subduction of the Bangong–Nujiang Ocean seafloor beneath the Lhasa Terrane. Tectonically, the crust of the northern Lhasa subterrane was shortened by >50% as a result of southward thrusting during a period from the Late Cretaceous to Paleocene (Kapp et al., 2003; Volkmer et al., 2007). The southern Lhasa subterrane also experienced crustal shortening during the Late Cretaceous–earliest Tertiary, as indicated by the widespread strongly deformed/shortened (>40%) pre-Cenozoic rocks unconformably overlain by the relatively undeformed Linzizong volcanic succession (Yin and Harrison, 2000; Mo et al., 2003, 2007, 2008; He et al., 2007; and references therein).

The SNMZ, which extends SE–NW for ~2000 km across the northern part of the present-day Lhasa Terrane (Fig. 1a), has been interpreted as representing a dismembered ophiolitic mélange zone associated with the evolution of a back-arc basin likely developed in the Early Cretaceous (Qu et al., 2003; Zhang et al., 2004; Baxter et al., 2009). The LMF shown as a large thrust fault extends for ~1500 km across the southern part of the present-day Lhasa Terrane (Fig. 1a), indicating that the Carboniferous–Permian metasedimentary sequence of the central Lhasa subterrane was thrust southward over the southern Lhasa suberrane during or prior to the India–Asia collision (Pan and Ding, 2004; He et al., 2007).

3. Field and petrographic observations

The samples were collected from the Lower Cretaceous Zenong Group volcano-sedimentary sequence and associated granitoids in Xainza, Coqen, Xungba, and Gar areas with a spatial coverage of ~900 km (from E80° to E89°) along the central Lhasa subterrane (Fig. 1b). Sample details are summarized in Table 1. The Zenong Group in the central Lhasa subterrane covers an area of ~2.0×10^4 km^2 from Nam Tso in the east to Gar to the west (Fig. 1b) with an average thickness of up to 1000 m (Zhu et al., 2006). The Zenong Group is dominated by felsic lavas and volcaniclastic rocks with minor andesites and rare outcrops of basalts. The andesite samples are porphyric with plagioclase (25–30%) and clinopyroxene (20–25%) phenocrysts. The dacite and rhyolite samples are porphyric with quartz (5–25%), alkali-feldspar (5–30%), plagioclase (10–30%) and minor biotite (3–5%) phenocrysts. The rhyolitic tuff sample (DXL1-3) contains pyroclastic detritus, vitric materials and volcanic ash as well as exotic carbonate fragments.

The Early Cretaceous granitoids are widespread in the central Lhasa subterrane (~1.6×10^4 km^2, Fig. 1b). These rocks intrude the Carboniferous–Permian metasedimentary sequence, the Nyainqêntanglha Group metamorphic rocks and the Zenong Group. These rocks consist mainly of granodiorite and monzogranite with abundant dioritic enclaves (see Fig. 2a and b). The host granodiorite is composed of plagioclase (30–45%), alkali-feldspar (10–20%), quartz (15–20%) and biotite (5%) with varying amounts of hornblende (3–15%). Accessory minerals include apatite, zircon, titanite and Fe–Ti oxides. The dioritic enclaves range from angular to oval in shape. Igneous textures include megacrysts of quartz, alkali-feldspar and oscillatory-zoned plagioclase (Fig. 2a and b), similar to textures described from mafic enclaves around the world (cf. Yang et al., 2007). Mafic minerals include hornblende and biotite. Accessory minerals include titanite, apatite, zircon and Fe–Ti oxides. As a whole, the volcanic rocks and granitoids show similar lithological association and petrographic features from Xainza to Coqen in the central Lhasa subterrane (Fig. 1b).

4. Analytical methods

Major element compositions of bulk rock samples were determined by XRF on fused glass disks in the State Key Laboratory of Continental Dynamics, Northwest University (Xi'an), with analytical uncertainties generally better than 5%. Bulk-rock trace element compositions were determined by ICP-MS (Elan 6100 DRC) after acid digestion of samples in Teflon bombs and dilution in 2% HNO_3 in the same laboratory. During analysis, data quality was monitored by repeated analyses of USGS rock reference materials (BHVO-2, BCR-2, AGV-1, and G-2, see Gao et al., 2002 for analytical details). Table A1 (where and in later sections the prefix "A" refers to tables and figures in appendices) gives the procedural blank and four USGS rock reference standards analyzed together with our samples. The accuracy is generally better than 10%, with many elements agreeing to within 2% of AGV-1 (andesite-USGS) and G-2 (granite-USGS) rock standards, with the exception of Ni, Gd and Ta in G-2, which differ by >20% from the reference values (Table A1).

Bulk-rock Nd and Sr isotopic compositions were determined using a Finnigan MAT-261 mass spectrometer operated in static mode at China University of Geosciences (Wuhan). Analytical details were given in Rudnick et al. (2004) and Liu et al. (2004). Sr and Nd isotopic fractionation was normalized to $^{86}Sr/^{88}Sr=0.1194$ and $^{146}Nd/^{144}Nd=0.7219$, respectively. The average $^{143}Nd/^{144}Nd$ ratio of the La Jolla standard measured during the sample runs is 0.511862 ± 5 (2-sigma), and the average $^{87}Sr/^{86}Sr$ ratio of the NBS987 standard is 0.710236 ± 16 (2-sigma). Total procedural Sr and Nd blanks are <1 ng and <50 pg, respectively. Table 1 gives the analytical data.

Zircons were separated for each sample from ~3 kg materials by heavy-liquid and magnetic methods in the Laboratory of the Geological Team of Hebei Province, China. Cathodoluminescence (CL) images were taken at the Institute of Geology and Geophysics, Chinese Academy of Sciences (Beijing) for inspecting internal structures of individual zircons and for selecting positions for U–Pb and Lu–Hf isotope analyses.

Zircon U–Pb age data were obtained using laser ablation inductively coupled plasma mass spectrometry (LA-ICPMS) at China

University of Geosciences (Wuhan) following Zhang et al. (2007a) and the sensitive high-resolution ion microprobe (SHRIMP) for sample GB-8 at the Beijing SHRIMP Center following Liu et al. (2006). During the SHRIMP U–Pb analysis, U–Th–Pb isotope ratios were measured relative to the zircon standard TEMORA (Black et al., 2003). During LA-ICPMS analysis, U–Th–Pb concentrations were calibrated using NIST SRM 610 as an external standard with ^{29}Si being internal standard. $^{207}Pb/^{206}Pb$ and $^{206}Pb/^{238}U$ ratios were calculated using GLITTER 4.0 (Jackson et al., 2004), which was then corrected using the Harvard zircon 91,500 as external standard. The $^{207}Pb/^{235}U$ ratio was calculated from the values of $^{207}Pb/^{206}Pb$ and $^{206}Pb/^{238}U$. Common lead was corrected for using the correction function (see Andersen, 2002). ISOPLOT (version 3.0) (Ludwig, 2003) was used for plotting concordia diagrams and age spectra, and for age calculations. The analytical details are given in Zhang et al. (2007a). Uncertainties on individual analyses are reported as 1-sigma; mean ages for pooled $^{206}Pb/^{238}U$ results are reported as 2 sigma's.

Zircon Hf isotope analyses were subsequently done on the same spots using LA-ICPMS with a beam size of 60 μm and laser pulse frequency of 8 Hz at the Institute of Geology and Geophysics, Chinese Academy of Sciences (Beijing). Details of instrumental conditions and data acquisition were given in Wu et al. (2006) and Ji et al. (2009a). During analysis, $^{176}Hf/^{177}Hf$ and $^{176}Lu/^{177}Hf$ ratios of the standard zircon (91,500) were 0.282322 ± 22 ($2\sigma_n$, $n=28$) and 0.000319, consistent with the values (0.282307 ± 31, $2\sigma_n$, $n=44$) obtained previously in this laboratory (Wu et al., 2006).

5. Analytical data

The bulk-rock compositional data are listed Table 1, and the zircon U–Pb and Lu–Hf isotopic data are given in Appendices (Tables A2, A3 and A4) and are summarized in Table 2.

5.1. Bulk-rock data

Bulk-rock geochemical analysis on a comprehensive sample suite is in progress. We report here the available data on twelve samples that include 10 silicic rocks and 2 intermediate rocks (andesite and dioritic enclave) (Table 1). On the basis of emplacement timing and zircon Hf isotopic compositions (see below), the silicic samples are divided into the 130–116 Ma and 110 ± 3 Ma (i.e., 112–107 Ma) groups.

The 130–116 Ma silicic rocks are of calc-alkaline type, ranging from dacite/granodiorite to rhyolite/granite with high SiO_2 (66–77 wt.%) (Fig. 3a). These rocks are metaluminous to peraluminous, with aluminum saturation index [i.e. A/CNK = molecular $Al_2O_3/(CaO + Na_2O + K_2O)$] of 0.95–1.23. The 110 ± 3 Ma silicic rocks have similar compositions (e.g., 65–75 wt.% SiO_2, 0.90–1.16 A/CNK) (Table 1). An enclave sample (NX5-3) from western Nixiong in Coqen area is dioritic (57.41 wt.% SiO_2) (Fig. 3a) with 3.64 wt.% MgO and $Mg^{\#}$ of 48. An andesite sample (SZ48) from Eyang in Xainza area has a similar composition (e.g., 60.47 wt.% SiO_2, 3.19 wt.% MgO, and $Mg^{\#}$ of 42) (Table 1).

Both 130–116 Ma and 110 ± 3 Ma silicic rocks display a weak to moderate negative Eu anomaly ($Eu/Eu^* = 0.32$–0.66, and 0.43–0.80, respectively) and are variably enriched in light rare earth elements (REEs) with $(La/Yb)_N$ of 4.9–14.7 and 7.6–9.3, respectively. The intermediate rocks have similar overall characteristics, e.g., $Eu/Eu^* = 0.74$ and $(La/Yb)_N = 4.7$ for dioritic enclave (NX5-3), and $Eu/Eu^* = 0.74$ and $(La/Yb)_N = 7.0$ for andesite (SZ48). In primitive mantle-normalized trace element diagram (Fig. 3b), both 130–116 Ma and 110 ± 3 Ma silicic rocks are enriched in large ion lithophile elements (LILEs; e.g., U, Th, and Rb) and light REEs, but relatively depleted in high field strength elements (e.g., Nb, Ta, and Ti), and elements reflecting plagioclase (e.g., Sr and Ba) and apatite (P) fractionation (Fig. 3b).

The 130–116 Ma silicic rocks are characterized by higher initial $^{87}Sr/^{86}Sr$ (0.7141–0.7209) and lower $\varepsilon_{Nd}(t)$ (-13.7 to -7.8) (with T_{2DM} model ages of 1.6–2.0 Ga) relative to the 110 ± 3 Ma silicic rocks that have initial $^{87}Sr/^{86}Sr$ of 0.7073–0.7138 and $\varepsilon_{Nd}(t)$ of -10.4 to -4.6 (with T_{2DM} model ages of 1.3–1.8 Ga) (Table 1). The intermediate rocks also have relatively high initial $^{87}Sr/^{86}Sr$ (0.7088–0.7148) and low $\varepsilon_{Nd}(t)$ (–9.9 to -7.8) within the range of the 110 ± 3 Ma silicic rocks (Table 1).

The new data reported here, in combination with the data on igneous rocks of Early Cretaceous age reported in the recent literature from different sites of the central Lhasa subterrane (Kang et al., 2008; Zhu et al., in press; Zhao et al., in press), are summarized in the form of histogram of A/CNK (Fig. 3c) and a diagram of A/CNK vs. U–Pb age (Fig. 3d). These two diagrams show several important features: (1) the rocks are mostly metaluminous ($A/CNK \leq 1.1$, corresponding to I-type granite), (2) the metaluminous (I-type) and strongly peraluminous (S-type) varieties are coeval (e.g., 130–107 Ma), (3) almost all the intrusive rocks are metaluminous except a granite (sample SZ39) that is peraluminous ($A/CNK = 1.13$) and shows apparently older emplacement age of ~125 Ma, and (4) overall, the igneous rocks tend to become progressively more metaluminous (or more mafic and less silicic) through time.

5.2. Zircon U–Pb isotopic results

Zircons from andesite and diorite enclave samples are mostly euhedral and show short prismatic forms (50–150 μm long) with an aspect ratio of 1:1–3:1 and clear oscillatory zoning. A few zircons show rounded or ovoid shapes and complex internal texture (Fig. A1a). Zircons from the more silicic rocks (including dacite, rhyolite, granodiorite and diorite) are mostly prismatic (100–300 μm long) with an aspect ratio of 2:1–4:1. These zircons are transparent, colorless to pale brown and show clear oscillatory zoning (Fig. A1b–1j). Note that zircons with complex internal textures observed in a diorite sample (Fig. A1j) are rare in silicic samples. All the analyzed zircons, excluding inherited cores, have varying uranium (65–3255 ppm) and thorium (64–4022 ppm) contents with Th/U ratio varying from 0.15 to 2.46 (Tables A2 and A3), consistent with their being of magmatic origin (Hoskin and Schaltegger, 2003). Thus, the interpretation of the zircon U–Pb isotopic data (see below) is straightforward and the obtained ages are interpreted as representing the timing of zircon crystallization and thus the timing of the host rock emplacement.

In the western part of the central Lhasa subterrane near Gar (Fig. 1b), twenty-one analyses of zircons from an andesite sample (SQ0666) yield a weighted mean $^{206}Pb/^{238}U$ age of 102 ± 1 Ma (Fig. A1a). To the east of Xungba in the central Lhasa subterrane (Fig. A1b), a rhyolite sample (GJ0611) gives an older zircon $^{206}Pb/^{238}U$ age of 143 ± 2 Ma (Fig. A1b). Zircons from another rhyolite sample (GJ0612) yield two weighted mean $^{206}Pb/^{238}U$ ages of 139 ± 1 Ma and 129 ± 1 Ma (Fig. A1c). The younger age (~129 Ma), identical to that of dacitic rocks of the lower Zenong Group northwest of Coqen (~130 Ma, Zhu et al., 2008c), is interpreted as the cooling age of the rhyolite melt in a pre-eruption magma chamber.

Five new silicic samples were dated from the central part of the central Lhasa subterrane around the Coqen area (Fig. 1b). A dacite sample (CMN04-2) collected from north of Bangdo yields a zircon $^{206}Pb/^{238}U$ age of 125 ± 1 Ma (Fig. A1d), similar to the dacitic rocks reported north of Daxiong (121 ± 1 Ma, Zhu et al., 2008c). Further northwestward of the above locality, zircons from a rhyolitic tuff (DXL1-3) yield a $^{206}Pb/^{238}U$ age of 112 ± 1 Ma (Fig. A1e), which is identical to the $^{206}Pb/^{238}U$ age of 111 ± 1 Ma obtained from a rhyolite (Zhu et al., 2008c) ~5 km southwest of Coqen (Fig. 1b). To the southeast of Coqen near Nixiong, a granodiorite sample from a drill core gives a zircon $^{206}Pb/^{238}U$ age of 116 ± 1 Ma (Fig. A1f). In the same locality, however, a host granodiorite (NX5-2) and a dioritic enclave (NX5-3) yield relatively younger but identical zircon $^{206}Pb/^{238}U$ ages of 109 ± 1 Ma, and 108 ± 1 Ma, respectively (Fig. A1g–1h).

Two new granitoid samples, including a host granodiorite (SZ08-3) and a dioritic enclave (SZ08-1), from the eastern part of the central

Table 1
Bulk-rock major, trace element and Sr–Nd isotopic data of the Early Cretaceous igneous rocks in the east–west transect along the central Lhasa subterrane, southern Tibet.

	DX2-1	DX13-1	DX19-1*	DX21-1	DXL1-3	NX5-2	NX5-3	GB-8	SZ39	SZ43	SZ48	SZ52
Rock type	Dacite	Dacite	Monzogranite	Rhyolite	Rhyolite	Granodiorite	Diorite enclave	Granodiorite	Granite porphyry	Rhyolite	Andesite	Dacite
Age (Ma)	130	121.3	107	111.6	111.5	108.4	108.6	116.3	125	129	111	107
XRF — major element (wt.%)												
SiO_2	66.48	68.05	71.10	75.30	73.95	67.52	57.41	68.43	76.58	72.66	60.47	64.97
TiO_2	0.75	0.58	0.35	0.10	0.14	0.51	0.78	0.29	0.06	0.22	0.77	0.57
Al_2O_3	15.15	14.74	14.53	13.48	10.94	15.36	16.38	13.66	12.39	14.29	15.02	14.66
TFe_2O_3	5.15	4.07	2.95	1.43	1.31	4.18	8.04	2.88	1.54	2.20	8.75	6.80
MnO	0.12	0.12	0.06	0.05	0.04	0.06	0.22	0.21	0.02	0.03	0.15	0.08
MgO	1.33	0.98	0.94	0.55	0.77	1.36	3.64	0.65	0.06	0.29	3.19	1.59
CaO	3.13	2.96	3.21	0.28	2.35	3.74	6.53	2.22	0.23	0.58	3.66	3.1
Na_2O	3.65	3.37	3.37	3.94	3.83	3.25	3.64	1.63	2.99	2.96	3.77	2.83
K_2O	2.76	2.93	2.81	4.23	1.41	2.92	2.04	7.07	5.22	5.21	2.16	2.54
P_2O_5	0.17	0.14	0.09	0.02	0.03	0.13	0.16	0.08	0.01	0.04	0.12	0.13
LOI	1.53	1.99	0.85	0.84	4.76	0.66	0.78	2.46	0.75	1.60	3.73	4.79
Total	100.22	99.93	100.26	100.22	99.53	99.69	99.62	99.58	99.52	99.53	99.57	99.86
Mg#	34.06	32.50	38.92	43.48	54.04	39.42	47.52	31.10	7.23	20.86	42.16	31.86
A/CNK	1.03	1.04	1.01	1.16	0.90	1.00	0.82	0.95	1.13	1.23	0.99	1.12
ICP-MS — trace element (ppm)												
Be	1.93	1.97	1.35	1.74	0.97	1.84	2.05	0.98	2.57	2.70	2.13	2.44
Sc	16.6	12.7	9.44	3.32	4.27	9.06	21.3	7.04	2.31	4.27	20.9	11.2
V	68.6	42.7	43.8	4.16	28.8	71.7	186	31.6	1.03	12.5	147	65.8
Cr	4.47	3.22	3.41	2.18	3.23	6.91	36.8	4.34	91.3	65.5	26.7	20.7
Co	8.72	6.34	4.28	1.13	2.26	7.91	18.4	2.14	0.96	1.10	17.80	7.64
Ni	3.66	2.73	1.98	1.67	2.97	4.03	8.42	1.88	1.37	1.10	7.91	3.88
Cu	11.0	6.84	5.62	2.52	10.6	4.51	14.1	12.1	1.22	2.95	19.8	9.10
Ga	16.7	18.1	15.0	12.7	11.1	15.6	17.6	11.4	13.3	16.4	15.1	16.4
Rb	103	109	96.0	126	57.2	106	80.1	264	194	167	83.5	131.5
Sr	194	175	231	49.9	79.2	260	261	114	53.4	160	273	124
Y	48.8	46.3	24.0	23.5	17.3	22.1	42.9	20.8	28.1	30.2	25.3	27.1
Zr	289	257	134	92.5	85.8	139	104	151	96.0	185	130	181
Nb	12.4	12.2	6.42	8.18	8.87	7.05	7.90	8.07	12.4	12.1	8.24	10.2
Cs	0.88	5.42	2.18	1.99	9.59	3.50	3.42	4.42	1.94	3.20	5.99	8.56
Ba	633	719	599	750	200	452	328	1280	355	1230	661	190

La	40.0	40.2	29.5	31.2	21.7	31.0	30.8	31.6	22.0	62.0	27.0	35.1
Ce	82.6	81.5	55.7	57.9	44.7	57.4	69.2	56.5	54.7	123	53.1	67.8
Pr	9.96	9.62	5.97	5.86	4.85	5.92	8.37	5.66	5.92	14.3	6.00	7.48
Nd	40.0	37.3	22.7	20.3	17.6	21.3	33.4	20.5	22.6	50.9	23.7	29.1
Sm	8.45	7.77	4.30	3.94	3.85	4.08	7.23	3.95	5.32	8.28	4.60	5.31
Eu	1.91	1.70	0.92	0.59	0.53	1.07	1.74	0.79	0.55	1.64	1.13	1.11
Gd	9.17	8.13	3.97	3.94	3.63	4.11	7.24	3.48	5.17	8.10	4.81	5.57
Tb	1.38	1.22	0.63	0.56	0.53	0.58	1.08	0.56	0.91	1.06	0.73	0.82
Dy	8.91	7.86	3.77	3.63	3.33	3.64	7.09	3.30	5.36	5.76	4.31	4.74
Ho	1.94	1.70	0.77	0.82	0.69	0.81	1.55	0.69	1.06	1.04	0.86	0.95
Er	5.46	4.79	2.35	2.52	1.97	2.35	4.60	2.10	3.01	3.00	2.55	2.77
Tm	0.76	0.67	0.36	0.39	0.29	0.34	0.68	0.34	0.46	0.42	0.39	0.41
Yb	4.95	4.43	2.40	2.81	2.06	2.39	4.71	2.25	3.24	3.03	2.76	2.90
Lu	0.72	0.66	0.37	0.44	0.30	0.36	0.71	0.35	0.49	0.44	0.43	0.43
Hf	7.90	6.73	3.57	3.06	2.81	3.62	2.95	3.84	4.13	5.56	3.80	5.01
Ta	1.09	1.05	0.58	1.09	1.22	0.81	0.81	0.89	1.40	1.07	0.78	1.07
Pb	16.0	17.4	12.9	4.75	26.9	12.2	12.6	184	27.4	28.7	19.7	14.4
Th	15.0	16.0	14.4	23.2	20.3	13.3	10.6	16.0	28.5	28.5	15.4	19.2
U	2.36	2.51	1.34	3.48	1.93	1.55	0.94	2.16	2.93	2.18	2.30	3.10
Sr–Nd isotope compositions												
$^{87}Rb/^{86}Sr$	1.5319	1.8002	1.2004	7.3458	2.0905	1.1834	0.8871	6.7105	12.5000	3.1820	0.8531	3.2840
$^{87}Sr/^{86}Sr$	0.71694	0.71765	0.70947	0.71985	0.71066	0.71129	0.71017	0.72673	0.74023	0.72677	0.71613	0.71876
2σ	0.000017	0.000013	0.000013	0.000021	0.000017	0.000016	0.000016	0.000017	0.000016	0.000018	0.000013	0.000017
$^{147}Sm/^{144}Nd$	0.12772	0.12573	0.11443	0.11774	0.13250	0.11585	0.13078	0.11641	0.1478	0.1027	0.1219	0.1164
$^{143}Nd/^{144}Nd$	0.51204	0.51203	0.51235	0.51216	0.51229	0.51217	0.51219	0.51218	0.51190	0.51189	0.51207	0.51205
2σ	0.000006	0.000007	0.000008	0.000006	0.000005	0.000008	0.000008	0.000008	0.000008	0.000006	0.000006	0.000008
$(^{87}Sr/^{86}Sr)i$	0.7141	0.7146	0.7076	0.7082	0.7073	0.7095	0.7088	0.7156	0.7180	0.7209	0.7148	0.7138
$(^{143}Nd/^{144}Nd)i$	0.51193	0.51193	0.51227	0.51207	0.51219	0.51208	0.51210	0.51209	0.51178	0.51180	0.51199	0.51197
$\varepsilon_{Nd}(t)$	−10.5	−10.7	−4.6	−8.3	−5.9	−8.1	−7.8	−7.8	−13.7	−13.1	−9.9	−10.4
T_{DM} (Ga)	2.0	2.0	1.2	1.6	1.6	1.5	1.8	1.5	2.9	1.7	1.8	1.7
T_{2DM} (Ga)	1.8	1.8	1.3	1.6	1.4	1.6	1.5	1.6	2.0	2.0	1.7	1.8

LOI = loss on ignition. $Mg\# = 100\times Mg^{2+}/(Mg^{2+}+TFe^{2+})$, $TFeO^* = 0.9\times TFe_2O_3$; A/CNK = molecular $Al_2O_3/(CaO+Na_2O+K_2O)$. Corrected formula as follows: $(^{87}Sr/^{86}Sr)_i = (^{87}Sr/^{86}Sr)_{sample} + {}^{87}Rb/^{86}Sr\,(e^{\lambda t}-1)$, $\lambda = 1.42\times10^{-11}\ a^{-1}$; $(^{143}Nd/^{144}Nd)_i = (^{143}Nd/^{144}Nd)_{sample} + (^{147}Sm/^{144}Nd)_m\times(e^{\lambda t}-1)$, $\varepsilon_{Nd}(t) = [(^{143}Nd/^{144}Nd)_{sample}/(^{143}Nd/^{144}Nd)_{CHUR}(t)-1]\times10^4$, $(^{143}Nd/^{144}Nd)_{CHUR}(t) = 0.512638-0.1967\times(e^{\lambda t}-1)$. $T_{DM} = 1/\lambda\times\ln\{1+[((^{143}Nd/^{144}Nd)_{Sample}-0.51315)/((^{147}Sm/^{144}Nd)_{Sample}-0.21317)]\}$, $\lambda_{Sm-Nd} = 6.54\times10^{-12}\ a^{-1}$; T_{2DM} is the two-stage Nd depleted-mantle model age calculated using the same assumption formulation as Keto and Jacobsen (1987). Data marked by * are from Zhou et al. (2008), and by ** are from Zhao et al. (in press).

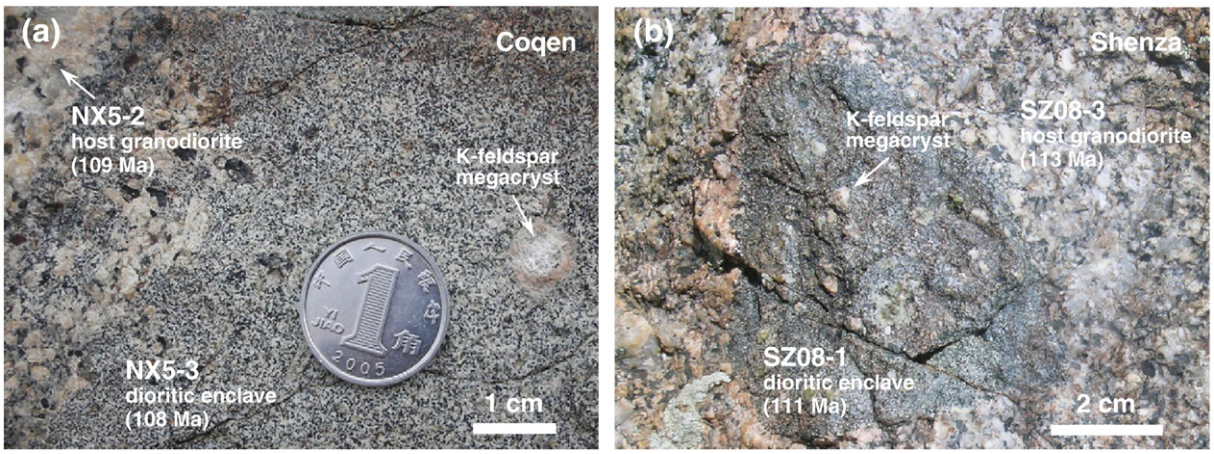

Fig. 2. Field photos showing mafic microgranular enclaves within granodiorite in Coqen (a) and Xainza (b) areas.

Lhasa subterrane around the Xainza area (Fig. 1b) were also dated. Eighteen U–Pb analyses for zircons from the host granodiorite give $^{206}Pb/^{238}U$ age of 113 ± 1 Ma (Fig. A1i), which is taken to represent the time of magmatic crystallization. Thirteen analyses of zircons from the dioritic enclave form a coherent group with a weighted mean $^{206}Pb/^{238}U$ age of 111 ± 1 Ma (Fig. A1j), within error of the age of the host granodiorite.

5.3. Zircon Lu–Hf isotopic results

A total of 203 zircons from 13 samples were analyzed for $^{176}Hf/^{177}Hf$ isotopic ratios (Table 2). The results are plotted in Fig. 4a (see Fig. A2 and Table A4 for details). The $\varepsilon_{Hf}(t)$ values (parts in 10^4 deviation of initial Hf isotope ratios between the zircon sample and the chondritic reservoir value), T_{DM} (the zircon Hf isotope mantle model ages) for intermediate rocks, and T_{DM}^{C} (the zircon Hf isotope crustal model ages based on a depleted-mantle source and an assumption that the protolith of the host magma has the average continental crustal $^{176}Lu/^{177}Hf$ ratio of 0.015) for silicic rocks were calculated following Griffin et al. (2002), using the ^{176}Lu decay constant adopted in Blichert-Toft and Albarède (1997). Our conclusions will not be affected if alternative decay constants are used.

Zircons from an andesite sample (SQ0666) in Gar area show exclusively positive $\varepsilon_{Hf}(t)$ of +1.2 to +6.0 (Fig. A2a). To the east of Xungba (Fig. 1b), magmatic zircons from two rhyolite samples (i.e., GJ0611, GJ0612) exhibit exclusively negative $\varepsilon_{Hf}(t)$ of −7.4 to −4.4 except an "outlier" grain from sample GJ0611 that shows the lowest negative value of −11.1 (Fig. A2b–2d).

In the Coqen area, zircon $\varepsilon_{Hf}(t)$ of three silicic samples older than 120 Ma (i.e., DX2-1, CMN04-2, DX13-1) show a relatively wide range from −14.2 to −4.8 (Fig. A2e–2g). In contrast, two silicic samples dated at ~110 Ma (i.e., DX21-1, DXL1-3) display small negative to positive zircon $\varepsilon_{Hf}(t)$ ranging from −5.4 to +3.4 (Fig. A2i–2j), which are also observed from a granodiorite of ~107 Ma (−1.0 to +3.0) reported recently in Daxiong pluton (Zhou et al., 2008). A granodiorite sample (GB-8) of ~116 Ma from a drill core near Nixiong exhibits small negative zircon $\varepsilon_{Hf}(t)$ (−7.1 to −3.0) (Fig. A2h). Zircons from the host granodiorite sample (NX5-2) show small negative $\varepsilon_{Hf}(t)$ (−6.2 to −2.1; Fig. A2k), within the range of zircon Hf isotopic composition of the dioritic enclave sample (NX5−3) that exhibits variable $\varepsilon_{Hf}(t)$ (−6.8 to −0.2; Fig. A2l).

In the Xainza area, with the exception of one zircon that shows the lowest negative value of −12.6, fourteen analyses of a dioritic enclave sample (SZ08-1) show uniform zircon $\varepsilon_{Hf}(t)$ of −6.7 to −4.5 (Fig. A2m), which are identical to those of the host granodiorite sample (SZ08-3) (−7.9 to −5.0; Fig. A2n). These zircon $\varepsilon_{Hf}(t)$ values, including the exceptional $\varepsilon_{Hf}(t)$ value (−12.6), are essentially similar to those of the contemporaneous silicic igneous rocks (e.g., SZ01-1, SZ07-1, SZ10-1, GRC02-1, GRC03-2) (Fig. 4a, Table 2) recently reported in Xainza area (Zhu et al., submitted for publication), suggesting that the Hf isotopic compositions of these silicic igneous rocks are very heterogeneous.

6. Discussion

6.1. Geochronology of the Early Cretaceous magmatism in the central Lhasa subterrane

Mapping projects involving detailed field studies revealed that the Early Cretaceous volcanic rocks and granitoids are widespread within the central Lhasa subterrane (Fig. 1b; Zhu et al., 2008b). However, the ages of these rocks (especially the granitoids) have often been questioned due to the lack of good quality age data. The recently obtained age data indicate that the Early Cretaceous magmatism in the Xainza area is concentrated between 129 and 107 Ma with a major emplacement age of ~112 Ma (Zhu et al., submitted for publication; Zhao et al., in press) (Fig. 1b). Such characteristics are further supported by radiometric dating on a host granodiorite (113 Ma) and a dioritic enclave (111 Ma) reported here (Table 2; Fig. 1b). To the west of the Coqen area in the central Lhasa subterrane, the geochronological data reported in this study (Table 2), in combination with published age data (Schwab et al., 2004; Volkmer et al., 2007; Zhu et al., 2008c; Zhou et al., 2008), suggest that the igneous rocks were mostly emplaced between 130 and 107 Ma with a major emplacement age of ~110 Ma, similar to the observations in the Xainza area. Further to the west, the age data obtained in this study and by Schwab et al. (2004) suggest that the magmatism took place during 143–116 Ma near Xungba, 126 Ma to the south of Gegyai, and 102 Ma near the Gar area (Fig. 1b).

In summary, the currently available age data (Table 2; Fig. 1b) show that (1) the central Lhasa subterrane experienced a long period of magmatism (from 143 to 102 Ma) throughout the Early Cretaceous, and (2) the magmatism intensified at ~110 Ma (Fig. 4b), which is coeval with the emplacement of the gabbroic intrusives in NW Daxiong (106 Ma; Liu et al., 2003), with host granites and mafic enclaves both in Xainza and Coqen areas of the central Lhasa subterrane. These results, together with the Early Cretaceous igneous rocks of 134–109 Ma widely distributed in the northern Lhasa subterrane (Booth et al., 2004; Kapp et al., 2007; Leier et al., 2007a; Zhu et al., submitted for publication, unpublished data) and of ~116–107 Ma scattered in the southern margin of the Qiangtang Terrane (e.g., north of Gerze; Kapp et al., 2005a) (Fig. 1b), reveal a magmatic flare-up at ~110 Ma (Fig. 4b) forming a linear zone along the strike (Fig. 1b).

Table 2
Summary of bulk-rock geochemical data, zircon U–Pb isotopic ages and Hf isotopic compositions of the Early Cretaceous igneous rocks in the east–west transect along the central Lhasa subterrane, southern Tibet.

No.[a]	Sample	Location	GPS position	Rock type	SiO_2 (wt.%)	A/CNK[b]	Age[c] (Ma)	$(^{87}Sr/^{86}Sr)i$	$\varepsilon_{Nd}(t)$	$\varepsilon_{Hf}(t)$	T_{DM} (Ga)	T_{DM}^{C} (Ga)	Reference[d]
1.	SQ0666	S Gar	N32°20.60′, E80°01.58′	Andesite	58.70	0.94	102 ± 1			+1.2 to +6.0	0.5–0.7	0.8–1.1	[1]
2.	GJ0611	E Xiongba	N32°02.42′, E82°12.04′	Rhyolite	74.39	1.08	143 ± 2			−11.1 to −4.4	1.0–1.3	1.5–1.9	[1]
3.	GJ0612	E Xiongba	N32°02.42′, E82°12.04′	Rhyolite	77.91	1.19	129 ± 1 139 ± 1			−7.3 to −4.8 −7.4 to −4.5	1.0–1.2 1.0–1.1	1.5–1.7 1.5–1.7	[1] [1]
4.	DX2-1	NW Daxiong	N31°27.51′, E84°56.08′	Dacite	66.48	1.03	130 ± 1*	0.71411	−10.5	−10.3 to −4.8	1.0–1.2	1.5–1.8	[1]
5.	DX13-1	N Daxiong	N31°30.08′, E85°10.72′	Dacite	68.05	1.04	121 ± 1*	0.71455	−10.7	−9.8 to −6.2	1.0–1.2	1.6–1.8	[1]
6.	DX19-1	E Dawa Tso	N31°16.91′, E85°07.57′	Monzogranite	71.10	1.01	107 ± 1	0.70765	−4.6	−1.0 to +3.0	0.7–0.8	1.0–1.2	[2]
7.	DX21-1	SW Coqen	N30°00.00′, E85°07.02′	Rhyolite	75.30	1.16	111 ± 1*	0.70820	−8.3	−5.4 to +0.2	0.8–1.0	1.2–1.5	[1]
8.	DXL1-3	N Daxiong	N31°39.31′, E85°11.70′	Rhyolite	73.95	0.90	112 ± 1	0.70734	−5.9	−0.2 to +3.4	0.7–0.8	1.0–1.2	[1]
9.	CMN04-2	N Bangdo	N31°21.05′, E85°54.49′	Rhyolite	70.44	1.14	125 ± 1			−14.2 to −11.2	1.2–1.4	1.9–2.1	[1]
10.	NX5-2	W Nixiong	N30°45.66′, E85°31.85′	Granodiorite	67.52	1.00	109 ± 1	0.70946	−8.1	−6.2 to −2.1	0.9–1.1	1.3–1.6	[1]
11.	NX5-3	W Nixiong	N30°45.66′, E85°31.85′	Diorite	57.41	0.82	108 ± 1	0.70880	−7.8	−6.8 to −0.2	0.8–1.1	1.2–1.6	[1]
12.	GB-8	W Nixiong (Hole sample)	N30°45.56′, E85°32.25′	Granodiorite	68.43	0.95	116 ± 1***	0.71639	−7.9	−7.1 to −3.0	0.9–1.1	1.4–1.6	[1]
13.	SZ39	Eyang	N30°49.71′, E87°55.84′	Granite porphyry	76.58	1.13	125 ± 1**	0.71802	−13.7	−13.9 to −11.1	1.2–1.5	1.9—2.1	[1]
14.	SZ43	Eyang	N30°49.94′, E87°55.82′	Rhyolite	72.66	1.23	129 ± 1**	0.72093	−13.1	−13.2 to −10.3	1.2–1.3	1.8–2.0	[1]
15.	SZ48	Eyang	N30°50.46′, E87°55.82′	Andesite	60.47	0.99	111 ± 1**	0.71478	−9.9	−9.5 to −3.0	0.9–1.2	1.4–1.8	[1]
16.	SZ52	Eyang	N30°50.46′, E87°55.82′	Dacite	64.97	1.12	107 ± 1**	0.71376	−10.4	−9.9 to +0.5	0.8–1.2	1.1—1.8	[1]
17.	GRC02-1	S Geren Tso	N31°03.98′, E88°12.41′	Dacite	64.61	1.13	114 ± 1			−13.9 to −3.7	0.9–1.3	1.4–2.1	[3]
18.	GRC03-2	S Geren Tso	N31°13.57′, E88°07.61′	Dacite	65.28	1.03	114 ± 1			−11.3 to −4.1	0.9–1.2	1.4–1.9	[3]
19.	SZ10-1	S Shenza	N30°53.40′, E88°39.74′	Dacite	64.45	1.35	112 ± 1			−7.3 to −4.2	0.9–1.1	1.4–1.6	[3]
20.	SZ08-1	SE Shenza	N30°46.37′, E88°50.63′	Diorite	57.62	0.92	111 ± 1			−12.6 to −4.5	1.0–1.3	1.5–2.0	[1]
21.	SZ08-3	SE Shenza	N30°46.37′, E88°50.63′	Granodiorite	67.12	0.99	113 ± 1			−7.9 to −5.0	1.0–1.1	1.5–1.7	[1]
22.	SZ07-1	SE Shenza	N30°45.96′, E88°54.08′	Dacite	63.51	1.04	111 ± 1			−8.5 to −4.2	0.9–1.1	1.4–1.7	[3]
23.	SZ01-1	SE Shenza	N30°45.38′, E88°55.34′	Dacite	64.81	0.82	117 ± 1**			−8.2 to −4.2	0.9–1.1	1.4–1.7	[3]

[a] 1 = Gar area; 2–3 = Xiongba area, 4–12 = Coqen area, 13–23 = Shenza area.
[b] A/CNK = molecular $Al_2O_3/(CaO + Na_2O + K_2O)$.
[c] *Age data cited from Zhu et al. (2008c), **Age data cited from Zhao et al. (in press); ***Dated by SHRIMP with 1σ uncertainty; others are dated by LA-ICPMS with 2σ uncertainty.
[d] [1] = this study; [2] = Zhou et al. (2008); [3] = Zhu et al. (submitted for publication).

6.2. Micro-continent nature of the central Lhasa subterrane

On the basis of the upper intercept age of discordant curve of U–Pb dating on zircons from Amdo orthogneiss, the pioneering work by Xu et al. (1985) identified the potential existence of Precambrian basement rock in the Amdo area of the Lhasa Terrane, which was verified later (Guynn et al., 2006). More recent studies suggested that the Lhasa Terrane is underlain by Early Proterozoic basement inferred from bulk-rock Nd isotope data of pre-Cenozoic siliciclastic rocks (Zhang et al., 2007b). Very recently, using a combined method of U–Pb and Lu–Hf isotope systematics on zircons from silicic rocks, Zhu et al. (submitted for publication) inferred the presence of ancient Archean basement with abundant Proterozoic juvenile crustal material in the central Lhasa subterrane.

As will be discussed below, isotopically, the intermediate rocks (including andesite and dioritic enclave) are largely mantle-derived and the silicic rocks are mainly derived from ancient/mature crust. Thus, only zircon Hf isotope crustal model ages (T_{DM}^{C}) are used for the silicic rocks to explore the basement (or crust) nature of the central Lhasa subterrane. The zircon Hf model ages of the silicic rocks obtained in this study and recent works (Zhou et al., 2008; Zhu et al., submitted for publication; Zhao et al., in press) (Table 2) are summarized in Fig. 5, illustrating a spatial variation of zircon Hf model ages extending ~E–W for 700 km from Gar in the west to Xainza to the east (E82°–E89°) in the central Lhasa subterrane. These data, together with the bulk-rock two-stage Nd model ages (T_{2DM}) (Table 1), show two important features: (1) zircons in the silicic rocks of 143–114 Ma from Xainza, Coqen and Xungba areas have similar T_{DM}^{C} ages ranging from 1.4 to 2.1 Ga with a peak at ~1.6 Ga, and (2) overall, the bulk-rock T_{2DM} ages and zircon T_{DM}^{C} ages of the Early Cretaceous silicic rocks in Coqen and Xainza areas appear to have

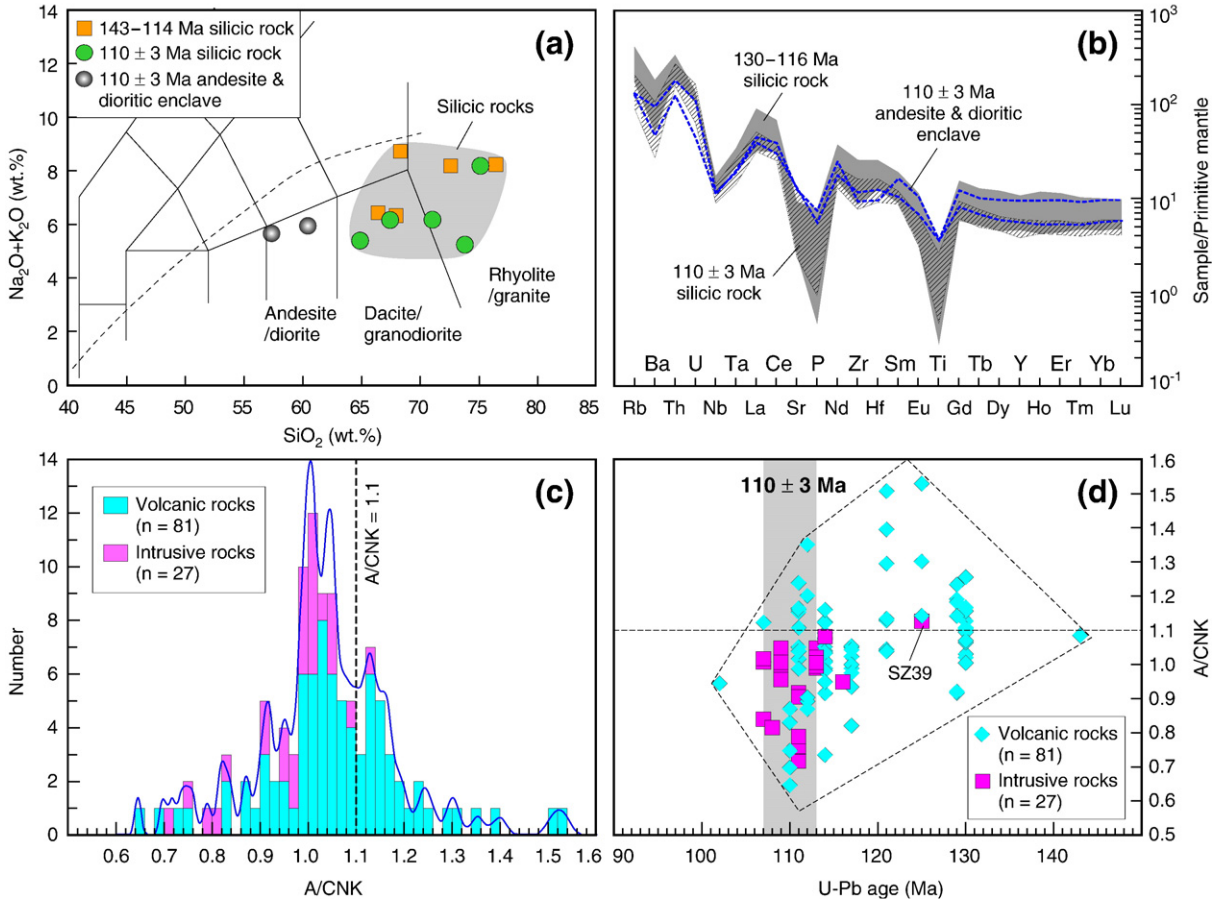

Fig. 3. (a) Plot of $Na_2O + K_2O$ vs. SiO_2. (b) Primitive-mantle-normalized trace element patterns for the Early Cretaceous igneous rocks in the central Lhasa subterrane. Data for normalization and plotting are from Sun and McDonough (1989). (c) Histogram of aluminum saturation index [i.e. A/CNK = molecular $Al_2O_3/(CaO + Na_2O + K_2O)$] of the Early Cretaceous igneous rocks in the central Lhasa subterrane (Kang et al., 2008, 2009; Zhao et al., in press; Zhu et al., in press). (d) A/CNK vs. U–Pb age plot of the Early Cretaceous igneous rocks in the central Lhasa subterrane.

become younger through time. These results suggest major stages of continental crust growth in the central Lhasa subterrane from the Paleoproterozoic to early Mesoproterozoic. Because zircon Hf model ages are calculated from $\varepsilon_{Hf}(t)$, and because crust–mantle interaction is inevitable, the measured $\varepsilon_{Hf}(t)$ values represent mixing between mantle-derived [large positive $\varepsilon_{Hf}(t)$] and ancient crust-derived [large negative $\varepsilon_{Hf}(t)$] materials. Hence, the $\varepsilon_{Hf}(t)$ for the re-worked crust is overestimated, and should be more negative and the "crustal" model age should be even older. Therefore, the continental crust of the central Lhasa subterrane should be formed before the Paleoproterozoic, which is in contrast to the southern Lhasa subterrane that is dominated by Phanerozoic juvenile materials (cf. Chu et al., 2006; Mo et al., 2007, 2008; Chiu et al., 2009; Ji et al., 2009a,b; Zhu et al., submitted for publication) and to the northern Lhasa subterrane that is dominated by late Mesoproterozoic to Neoproterozoic juvenile materials (Zhu et al., submitted for publication, unpublished data). Given that the study areas (Xainza, Coqen, and Xungba) can represent the entire central Lhasa subterrane (>700 km long, E82° to E89° and a ~100 km wide; Fig. 1b), we propose that the central Lhasa subterrane, which is separated to the south by the Luobadui–Milashan Fault (LMF) that correlates in space with a newly recognized Carboniferous–Permian suture zone (Yang et al., 2009) and to the north by the Shiquanhe–Nam Tso Mélange Zone (SNMZ) that may record the evolution of a back-arc basin likely developed in the Early Cretaceous (Qu et al., 2003; Baxter et al., 2009) (Fig. 1b), is effectively a micro-continental block with ancient basement during its journey from Gondwana to Eurasia across the Tethyan Ocean basins during the Mesozoic.

6.3. Origin of the Early Cretaceous magmatism in the central Lhasa subterrane

As presented above, the 130–116 Ma silicic rocks in the central Lhasa subterrane have high SiO_2 (>66 wt.%), high initial $^{87}Sr/^{86}Sr$ (0.7141–0.7209), and negative $\varepsilon_{Nd}(t)$ (−13.7 to −7.8). These features, together with the negative zircon $\varepsilon_{Hf}(t)$ values (−14.2 to −3.0) and ancient T_{DM}^{C} ages (1.4–2.1 Ga) (Table 2), indicate that these rocks were derived from anatexis of ancient continental crust. By contrast, the 110 ± 3 Ma silicic rocks (SiO_2 > 64 wt.%) exhibit varying initial $^{87}Sr/^{86}Sr$ (0.7073–0.7138) and $\varepsilon_{Nd}(t)$ (−10.4 to −4.6), and a wide range of zircons $\varepsilon_{Hf}(t)$ (−9.9 to +3.4) and T_{DM}^{C} ages (0.8–2.0 Ga) (Table 2), suggesting that these rocks were largely derived from anatexis of ancient crustal materials. The intermediate rocks (including andesite and dioritic enclave) have high initial $^{87}Sr/^{86}Sr$ (0.7088–0.7148) and low $\varepsilon_{Nd}(t)$ (−9.9 to −7.8), similar to those of the andesites (0.7056–0.7149) erupted on a thickened crust in the central Andes, where extensive crustal modification of the mantle-derived magmas took place (c.f., Davidson et al., 1993; Ramos, 1999). The bulk-rock Sr and Nd isotopic compositions, together with the negative zircon $\varepsilon_{Hf}(t)$ (−9.5 to −0.2) (Table 1), enable us to suggest that the intermediate rocks are the products of mantle-derived magmas contaminated by ancient crustal materials within the Lhasa micro-continental block.

It should be noted that there is a significant change in bulk-rock Sr and Nd isotopic composition (with the exception of sample SZ52) and zircon $\varepsilon_{Hf}(t)$ from the 110 ± 3 Ma rocks to the older (i.e., 143–114 Ma)

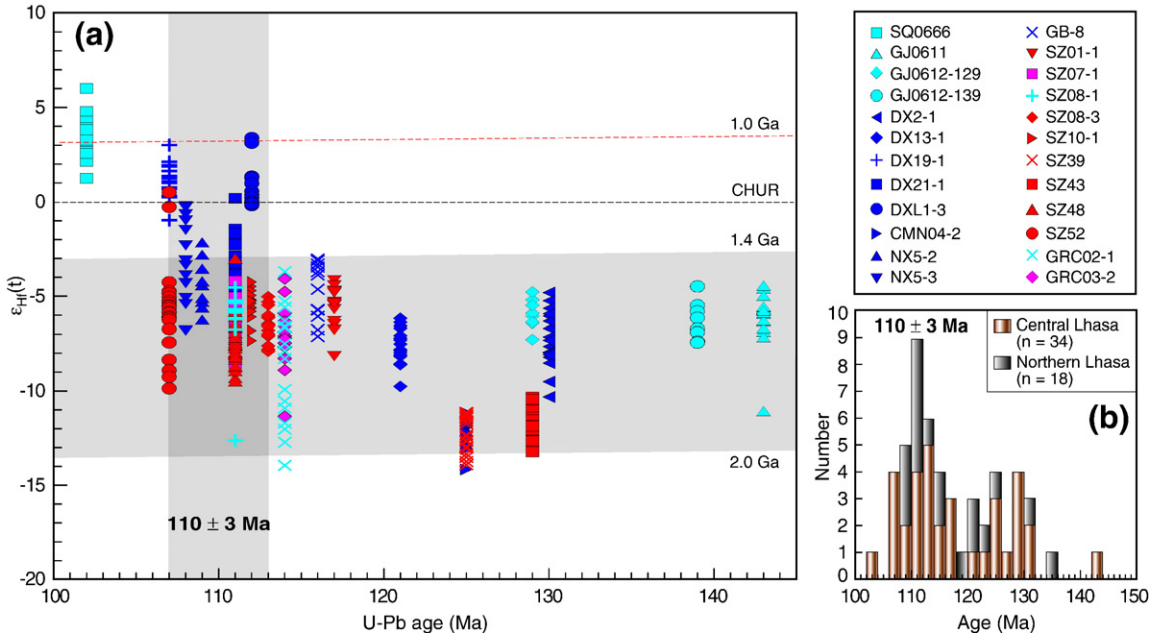

Fig. 4. (a) Plots of $\varepsilon_{Hf}(t)$ (parts per 10^4 deviation of initial Hf isotope ratios between zircon samples and the chondritic reservoir) vs. ages of the Early Cretaceous igneous rocks along the east–west transect throughout the central Lhasa subterrane. (b) Histogram of age dates for the Early Cretaceous igneous rocks in the central and northern Lhasa subterranes. Sources of age dates are the same as in Fig. 1.

rocks (Fig. 4a). This points to an increased contribution of a mantle component in the generation of the Early Cretaceous igneous rocks in the central Lhasa subterrane at ~110 Ma. Furthermore, the emplacement of abundant dioritic enclaves of ~110 Ma in Coqen and Xainza areas (Fig. 2a and b) and the contemporaneous gabbroic intrusives in the NW Daxiong area (Liu et al., 2003) also points to an increase in mantle-derived magmatism at that time. Therefore, our new bulk-rock Sr and Nd isotopic data and zircon U–Pb and Hf isotopic data, together with geological observations, document a significant change of magma source components at ~110 Ma, adding to our understanding of the history of Early Cretaceous magmatism in the central and northern Lhasa subterranes.

6.4. Early Cretaceous tectonomagmatic evolution of the Lhasa Terrane

6.4.1. Existing models for the generation of the Early Cretaceous magmatism

Previously, the Cretaceous igneous rocks in the central and northern Lhasa subterranes are interpreted as the products of crustal anatexis in response to crustal thickening during/or postdating the Lhasa–Qiangtang collision (Xu et al., 1985; Pearce and Mei, 1988) or high-temperature crustal melting due to asthenosphere upwelling after the Lhasa–Qiangtang collision (Harris et al., 1990). Recently, Chiu et al. (2009) argued in support of Pearce and Mei (1988) but emphasized the role of the northward subduction of the Neo-Tethyan Ocean seafloor. These three interpretations invoking syn- or post-orogenic collapse, however, fail to account for the significant change of magma source components at ~110 Ma documented for the first time in this study. In addition, there is a consensus that continental crust materials would not melt unless there exist excess K, U and Th as heat source, which is generally associated with an overthickened crust in a post-collisional intracrustal setting where mantle-derived magma is rare (cf. Sylvester, 1998). In the case of the central Lhasa subterrane, significant contributions of mantle-derived melts recorded in the silicic rocks of ~110 Ma and the coeval mantle-derived magmas documented in NW Daxiong (Liu et al., 2003; Zhang et al., 2004), northern Eyang (Kang et al., 2008), and southern Xainza (Zhu et al., in preparation) (Fig. 1b) clearly support the argument that the Early Cretaceous silicic igneous rocks were genetically associated with seafloor subduction and mantle basaltic magmatism.

Under the subduction-related framework, a popular interpretation, which is referred to here as the "traditional" model, is that the Cretaceous magmatism in the central and northern Lhasa subterranes (Fig. 1b) was generated by flat or low-angle northward subduction of the Neo-Tethyan Ocean seafloor (Fig. 6a) (e.g., Coulon et al., 1986; Copeland et al., 1995; Ding et al., 2003; Zhang et al., 2004; Kapp et al., 2005a, 2007; Chu et al., 2006; DeCelles et al., 2007; Leier et al., 2007a,b). In this traditional model, the significant change of magma source components at ~110 Ma and the shift of sedimentary environment from a peripheral foreland basin (related to the Lhasa–Qiangtang collision) to a back-arc rifting basin of the Gangdese arc during the beginning of the Aptian period (125–112 Ma) (Zhang et al., 2004; DeCelles et al., 2007; Leier et al., 2007b) can be explained by the slab rollback of the Neo-Tethyan Ocean floor (Fig. 6b). It should be pointed out that the interpretation of low-angle northward subduction of the Neo-Tethyan Ocean seafloor was originally proposed based on the assumption that magmatism was absent from 115 Ma to ca. 80 Ma in the Lhasa Terrane (Coulon et al., 1986). Subsequent studies also argued for this interpretation by assuming the scarcity of the Early Cretaceous igneous rocks in the southern Lhasa subterrane (see Kapp et al., 2007). However, recent studies revealed that the Early Cretaceous igneous rocks with arc-lava signatures (137–100 Ma) are present in the southern Lhasa subterrane (Wen et al., 2008; Zhu et al., 2008b, 2009a; Ji et al., 2009a,b). In addition, abundant 130–100 Ma detrital zircons with positive $\varepsilon_{Hf}(t)$ values in sedimentary rocks from the Xigaze fore-arc basin immediately north of the Indus–Yarlung Zangbo Suture Zone (IYZSZ) (Fig. 1b) are most likely sourced from the Gangdese arc during the fore-arc deposition (Wu et al., submitted for publication). These recently obtained data of detrital zircons further suggest that the Early Cretaceous magmatism in the southern Lhasa subterrane was more active and widespread than previously thought. These observations are inconsistent with the traditional low-angle or flat subduction model with which the poorly developed mantle wedge would not favor active and widespread magmatism in the southern Lhasa subterrane (Coulon et al., 1986; Gutscher et al., 2000). Thus, we contend that the shifts of magmatic nature (this study) and sedimentary environment (Zhang et al., 2004; Leier et al., 2007b) during the Aptian

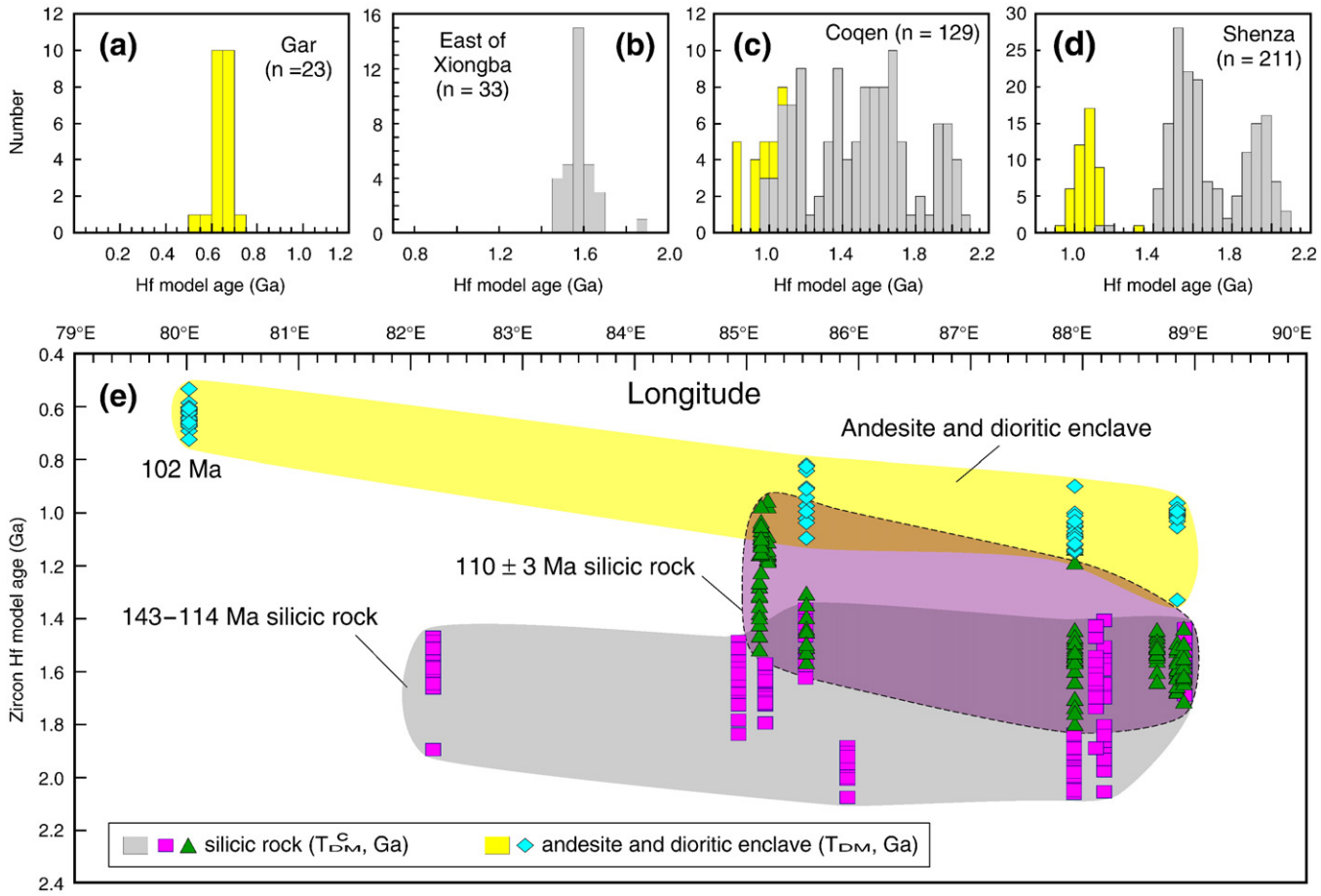

Fig. 5. (a–b–c–d) Histograms of Hf isotope model age for zircons from the Early Cretaceous igneous rocks from different sites of the central Lhasa Terrane. (e) Hf isotope model ages plotted against longitude of sample locations for the Early Cretaceous igneous rocks along the east–west transect in the central Lhasa subterrane.

cannot be attributed to the rollback of the low-angle or flat northward subduction of the Neo-Tethyan Ocean floor (Fig. 6b).

An alternative model involves the southward subduction of the Bangong–Nujiang Ocean floor for the generation of the Early Cretaceous igneous rocks in the central and northern Lhasa subterranes. Previously, a relatively small and short-lived Bangong–Nujiang Ocean was invoked to explain the volumetrically insignificant igneous rocks in the southern Qiangtang Terrane (cf. Dewey et al., 1988). Recently, Baxter et al. (2009), working on radiolarians from cherts in the Lagkor Tso ophiolitic mélange (Fig. 1b), proposed that the Bangong–Nujiang Ocean was never substantial. We note that the Bangong–Nujiang suture zone was considered by Baxter et al. (2009) to be very diffuse and very wide especially from Dongqiao to Xainza (>200 km wide) (Fig. 1b). This interpretation fails to account for 1) the occurrence of the 120–110 Ma granitoids in Baingoin area because these rocks have negative bulk-rock $\varepsilon_{Nd}(t)$ (cf. Mo et al., 2005) and negative zircon $\varepsilon_{Hf}(t)$ (our unpublished data) that require the existence of a Mesoproterozoic basement; and 2) the extensive subduction-related Early Cretaceous magmatism (134–109 Ma) (Zhu et al., 2006, 2008b, submitted for publication, unpublished data; Kang et al., 2009) that is located in the northern Lhasa subterrane (i.e., the Bangong–Nujiang suture zone of Baxter et al., 2009) and is coeval with the radiolarians in the Lagkor Tso ophiolitic mélange (~131–121 Ma) (Baxter et al., 2009) (Fig. 1b).

In contrast to the above views, numerous studies argued for the existence of the Bangong–Nujiang Ocean although the timing of its opening and closure and the polarity of subduction of its seafloor remains hotly debated (Sengör, 1979; Allègre et al., 1984; Yin and Harrison, 2000; Kapp et al., 2003, 2005a, 2007; Qiu et al., 2004; Pan and Ding, 2004; Guynn et al., 2006; Pan et al., 2006; Shi, 2007; Zhu et al., 2009b). The very limited occurrence of igneous rocks in the southern Qiangtang Terrane led Allègre et al. (1984) to suggest that southward (rather than northward) subduction of the Bangong–Nujiang Ocean floor may have occurred in the northern Lhasa subterrane during the Mesozoic. We argue for this suggestion to explain the Early Cretaceous tectonomagmatic evolution of the central and northern Lhasa subterranes (see below) (Fig. 6c) because 1) the extensive subduction-related Early Cretaceous magmatism (134–109 Ma) are located in the northern Lhasa subterrane (Fig. 1b); 2) the apparent southward (i.e., continentward) decrease in $\varepsilon_{Hf}(t)$ of zircons of the Early Cretaceous silicic rocks from Nyima via Siling Tso to Xainza across the northern and central Lhasa subterranes (Zhu et al., submitted for publication) (Fig. 1b) is similar to the variation of bulk-rock $\varepsilon_{Nd}(t)$ in other continental margin batholiths (e.g. Sierra Nevada and Peninsular Ranges in California) (DePaolo et al., 2008) where continentward subduction occurred. Although our knowledge on the nature of the ~110 Ma mantle-derived magmas with potential involvement of asthenospheric components in the central Lhasa subterrane remains limited, the current data allow us to define a pattern for the coeval mafic magmatism as a linear trend with limited extent, which likely runs parallel to the strike from NW Daxiong (Liu et al., 2003; Zhang et al., 2004), via northern Eyang (Kang et al., 2008), to southern Xainza (Zhu et al., in press) (gray stars shown in Fig. 1b) along the northern part of the central Lhasa subterrane. These characteristics are similar to what is predicted by the slab break-off model, i.e. a narrow, linear zone of magmatism of limited extent with asthenospheric components when the subducted oceanic lithosphere slab had been detached from the adherent continental lithosphere as a result of gravitational resettling and strain localization (Davies and von

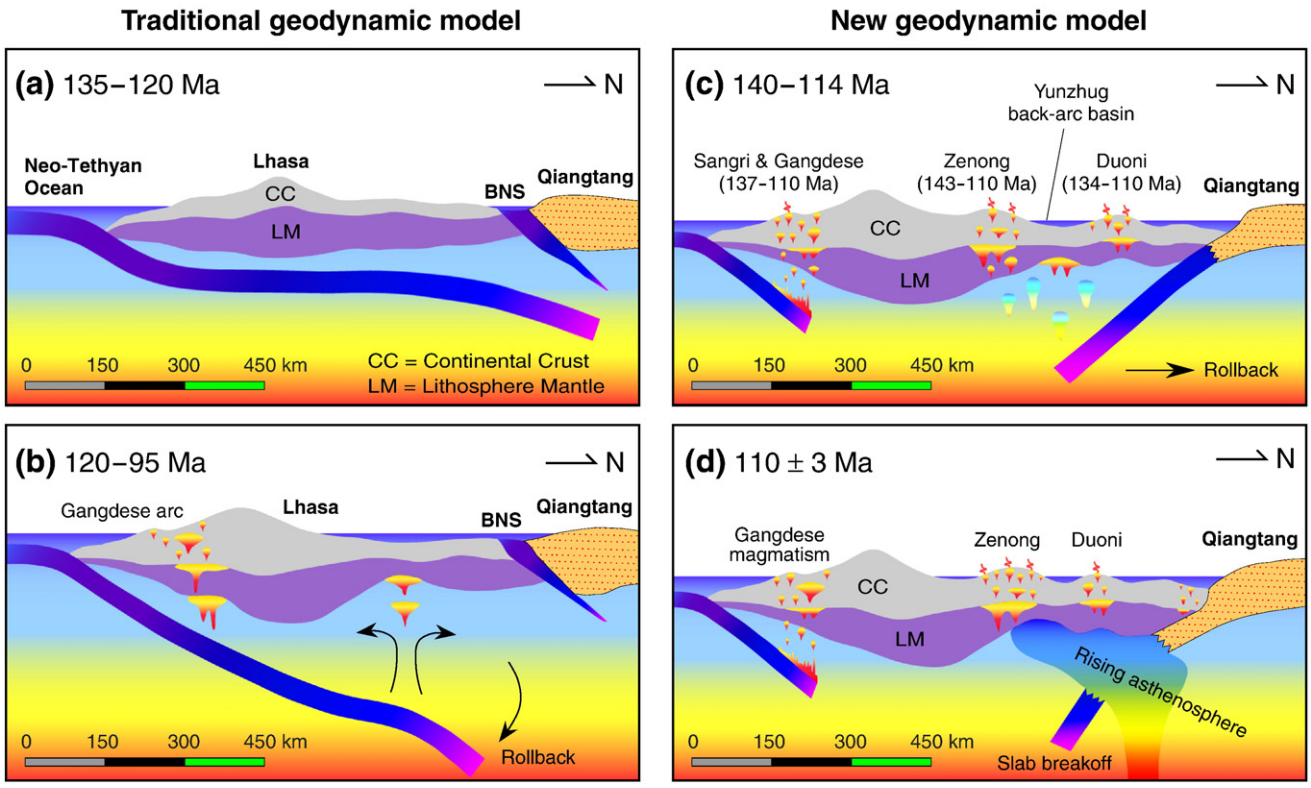

Fig. 6. Schematic illustrations of the nature and tectonomagmatic evolution of the Lhasa Terrane during the Mesozoic, illustrated by the north–south cross sections through time. a and b modified from Zhang et al. (2004); c and d modified from Zhu et al. (submitted for publication).

Blanckenburg, 1995; von Blanckenburg and Davies, 1995; Turner et al., 1999). Therefore, under the southward subduction-related setting of the Bangong–Nujiang Ocean floor, we propose that the slab break-off is a most probable mechanism to trigger the significant change of magma source components at ~110 Ma in the central Lhasa subterrane, although more data and further effort are needed to verify this model.

6.4.2. A new tectonomagmatic evolution model for the Lhasa Terrane during the Early Cretaceous

The data obtained in this study and in the literature, together with the foregoing discussion, lead us to propose a new tectonomagmatic evolution model, involving the southward subduction of the Bangong–Nujiang Ocean floor in the north and the northward subduction of the Neo-Tethyan Ocean floor in the south (Fig. 6c), for the Lhasa Terrane during the Early Cretaceous. Restoration of the ~50% Late Cretaceous and Cenozoic shortening in the Lhasa Terrane (Burg et al., 1983; Kapp et al., 2007) suggests that the whole Lhasa Terrane was probably >600 km wide during the Early Cretaceous. This means that the Lhasa Terrane itself can provide room to accommodate the two subducting/subducted slabs in the asthenosphere beneath the Lhasa Terrane. We start our new model from 140 Ma because the older magmatic records, such as the ~190 Ma andesitic rocks identified south of Yanhu in the northern Lhasa subterrane, and the ~185 Ma monzogranites identified north of Bangdo in the central Lhasa subterrane (our unpublished data) require further verification. Thus, the tectonomagmatic evolution in the Lhasa Terrane before 140 Ma remains uncertain.

A major change in the tectonic environment in the present-day southern Tibetan Plateau during the Mesozoic is the Lhasa–Qiangtang collision that was generally considered as having initiated during the late Jurassic–earliest Cretaceous and subsequent collision was diachronous along the Bangong–Nujiang suture zone (earlier in the east and later in the west) (Dewey et al., 1988; Yin and Harrison, 2000; Zhang et al., 2004; Kapp et al., 2005a, 2007; Leier et al., 2007b). In such a collisional setting, mantle-derived melts induced by the southward subduction of the Bangong–Nujiang Ocean seafloor would cause the anatexis of ancient continental crust materials of the central Lhasa subterrane (Fig. 6c). As the heat is carried by mantle-derived melts, the resulting felsic magmas are always mixtures of melts of existing crustal materials and mantle melts, explaining the coexistence of S-type (more crustal source) and I-type (significant mantle input) melts (this study) (Fig. 3d). During this stage, the northward subduction of the Neo-Tethyan Ocean seafloor beneath the southern Lhasa subterrane would lead to the emplacement of magmatism represented by the Lower Cretaceous Sangri Group (Zhu et al., 2006, 2009a) and Gangdese batholiths (130–80 Ma; Chung et al., 2005; Wen et al., 2008, Ji et al., 2009a,b) (Fig. 6c). With continued southward subduction of the Bangong–Nujiang Ocean seafloor, gravitational sinking had led to slab rollback at some time during the Early Cretaceous (Fig. 6c). This rollback would have led to the rifting and extension within the overriding plate of the central and northern Lhasa subterranes, and facilitated asthenospheric upwelling (Royden, 1993; Treloar et al., 1996), decompression mantle melting and subsequent mantle melt induced crustal melting. As a result, the surface sedimentary environment would have changed from dominantly non-marine clastic deposition in the Berriasian–Aptian period (130–112 Ma) to extensive shallow marine carbonate deposition (i.e., Langshan Formation) in the Aptian–Albian period (125–100 Ma) in a back-arc region, allowing the development of a series of back-arc basins along the Shiquanhe–Nam Tso Mélange Zone (SNMZ) (e.g., the Yunzhug, Asa, and Lagkor Tso back-arc basins) at that time (Qu et al., 2003; Pan and Ding, 2004; Zhang et al., 2004; Ye et al., 2005; Pan et al., 2006; Baxter et al., 2009) (Fig. 6c).

Recent stratigraphy and sedimentology studies along the Bangong–Nujiang suture zone revealed a transition from marine to nonmarine conditions between ca. 125 Ma and ca. 118 Ma in the Nyima area (Kapp et al., 2007). This means that the Qiangtang Terrane may have arrived at the trench and subsequently collided with the northern Lhasa

subterrane at about this time, resulting in the final closing of the Bangong–Nujiang Ocean. This final closing would be accompanied by continental lithosphere (i.e., the Qiangtang Terrane) subduction dragged by its subducted/subducting oceanic leading edge. The latter would continue to sink because of the negative buoyancy, but the buoyant continental lithosphere would not. The different behaviors of oceanic and continental portions of the same lithosphere will ultimately lead to the "slab" break-off (Fig. 6d) (von Blanckenburg and Davis, 1995; Wong et al., 1997). The break-off "window" would induce invasion of the deep asthenosphere into the mantle wedge, causing mantle decompression melting with the mantle-derived melt causing crustal anatexis in the ancient basement of the central Lhasa subterrane and/or thickened crust in response to the Lhasa–Qiangtang collision. This sequence of events as a result of the slab break-off ultimately led to a zonal magmatic flare-up with strong input of mantle-derived materials at ~110 Ma, possibly including the limited occurrence of ~110 Ma igneous rocks in the southern margin of the Qiangtang Terrane (Kapp et al., 2005a) (Fig. 1b), as the Lhasa Terrane may have amalgamated with the Qiangtang Terrane at this time. Our slab break-off may postdate the arrival of the Qiangtang Terrane at the trench by 8–15 Ma, corresponding well with thermo-mechanical modeling showing that the most favorable time interval for slab break-off is within 10–15 Myrs, after the arrival of continental material at the trench (Macera et al., 2008).

We note that structural geology studies undertaken in the Shiquanhe, northern Coqen, and Nyima areas of the central and northern Lhasa subterranes indicated a southward obduction of elements from the Bangong–Nujiang suture zone onto the Lhasa Terrane (Murphy et al., 1997; Yin and Harrison, 2000; Kapp et al., 2003, 2005a, 2007; Volkmer et al., 2007). It should be pointed out that south directed thrusting away from the Bangong–Nujiang suture zone may have occurred during the Late Cretaceous to Paleocene in a "thin-skinned" style that is concentrated in supracrustal assemblages (Kapp et al., 2003, 2005b; Volkmer et al., 2007). These structural data are not in conflict with the southward subduction of the Bangong–Nujiang Ocean floor (Fig. 6c and d). Because such a southward subduction may have ceased due to the absence of oceanic floor pull, and the region may have shifted from an active continental margin into an intracontinental setting. The Lhasa Terrane may have then experienced a northward underthrusting driven by the ongoing northward subduction of the Neo-Tethyan Ocean floor beneath the southern Lhasa subterrane since 110 Ma.

If our model is reasonable, the final amalgamation between the Qiangtang Terrane and the Lhasa Terrane would have occurred at 110 ± 3 Ma, which is compatible with the development of regional angular unconformity between the Late Cretaceous strata and their underlying strata (see Kapp et al., 2005a, 2007; Pan et al., 2006). We therefore propose that much of the Early Cretaceous igneous rocks in the central and northern Lhasa subterranes resulted from the southward subduction of the Bangong–Nujiang Ocean seafloor in a syncollisional setting (140–110 Ma) related to the Lhasa–Qiangtang collision. This scenario is comparable to the early Cenozoic magmatism in the southern Lhasa subterrane in response to the India–Asia collision (~65–40 Ma; Mo et al., 2008).

7. Conclusions

1) The central Lhasa subterrane experienced a long period of magmatism in the Early Cretaceous (~143–102 Ma) with a zonal magmatic flare-up at ~110 Ma. The latter is coeval with the emplacement of granites with abundant dioritic enclaves and rare outcrops of mafic rocks in this terrane.
2) The Early Cretaceous silicic rocks in the central Lhasa subterrane are metaluminous to peraluminous, enriched in Rb, Th, and U, and depleted in Ba, Nb, Ta, Sr, P, and Ti. These rocks have variable initial $^{87}Sr/^{86}Sr$ (0.7073–0.7209), negative $\varepsilon_{Nd}(t)$ (-13.7 to -4.6), and negative to positive $\varepsilon_{Hf}(t)$. The andesite and dioritic enclaves are characterized by initial $^{87}Sr/^{86}Sr$ (0.7088–0.7148), $\varepsilon_{Nd}(t)$ (-9.9 to -7.8), and negative zircon $\varepsilon_{Hf}(t)$ (-9.5 to -0.2) similar to those of the 110 ± 3 Ma silicic rocks.
3) The bulk-rock Sr and Nd isotopic data and zircon $\varepsilon_{Hf}(t)$ values indicate an increased contribution of a mantle component in the generation of the Early Cretaceous igneous rocks in the central Lhasa subterrane at ~110 Ma.
4) The central Lhasa subterrane with an ancient basement is probably a micro-continental block (i.e. the Lhasa micro-continental block), which explains the bulk-rock chemical and zircon Hf isotopic compositions of the silicic rocks as a result of deep crustal anatexis intimately triggered by subduction-related mantle melts in the Early Cretaceous.
5) The magmatic flare-up with strong input of mantle-derived materials at ~110 Ma can be explained by the break-off of the southward subduction of the Bangong–Nujiang Ocean seafloor during the Lhasa–Qiangtang collision.

Acknowledgements

The research was financially supported by the China Postdoctoral Special Science Foundation (to Di-Cheng Zhu), the National Key Project for Basic Research of China (Project 2006CB701402, 2009CB421002), the National Natural Science Foundation of China (40830317, 40973026, and 40873023), the Chinese 111 Project (No. B07011), and the programme of the Integrated Study of Basic Geology of Qinghai–Tibetan Plateau of the China Geological Survey. Yaoling Niu thanks a Leverhulme Trust for a Research Fellowship. We thank Ke-Qing Zong, Chen-Guang Sun for helping with the LA-ICPMS analyses; Paul Kapp and an anonymous reviewer for their constructive reviews that greatly improved the quality of this manuscript.

Appendix A. Supplementary data

Supplementary data associated with this article can be found, in the online version, at doi:10.1016/j.chemgeo.2009.09.008.

References

Allègre, C.J., Courtillot, V., Tapponnier, P., other 32 co-authors, 1984. Structure and evolution of the Himalaya–Tibet orogenic belt. Nature 307, 17–22.
Andersen, T., 2002. Correction of common lead in U–Pb analyses that do not report ^{204}Pb. Chemical Geology 192, 59–79.
Baxter, A.T., Aitchison, J.C., Zyabrev, S.V., 2009. Radiolarian age constraints on Mesotethyan ocean evolution, and their implications for development of the Bangong–Nujiang suture, Tibet. Journal of the Geological Society 166, 689–694.
Black, L.P., Kamo, S.L., Allen, C.M., Aleinikoff, J.N., Davis, D.W., Korsch, R.J., Foudoulis, C., 2003. TEMORA 1: a new zircon standard for Phanerozoic U–Pb geochronology. Chemical Geology 200, 155–170.
Blichert-Toft, J., Albarède, F., 1997. The Lu–Hf geochemistry of chondrites and the evolution of the mantle–crust system. Earth and Planetary Science Letters 148, 243–258.
Booth, A.L., Zeitler, P.K., Kidd, W.S.F., Wooden, J., Liu, Y.P., Idleman, B., Hren, M., Chamberlain, C.P., 2004. U–Pb zircon constraints on the tectonic evolution of Southeastern Tibet, Namche Barwa area. American Journal of Science 304, 889–929.
Burg, J.P., Proust, F., Tapponnier, P., Ming, C.G., 1983. Deformation phases and tectonic evolution of the Lhasa block (southern Tibet, China). Eclogae Geologica Helvetica 76, 643–665.
Chiu, H.Y., Chung, S.L., Wu, F.Y., Liu, D.Y., Liang, Y.H., Lin, Y.J., Iizuka, Y., Xie, L.W., Wang, Y.B., Chu, M.F., 2009. Zircon U–Pb and Hf isotope constraints from eastern Transhimalayan batholiths on the precollisional magmatic and tectonic evolution in southern Tibet. Tectonophysics. doi:10.1016/j.tecto.2009.02.034.
Chu, M.F., Chung, S.L., Song, B., Liu, D.Y., O'Reilly, S.Y., Pearson, N.J., Ji, J.Q., Wen, D.J., 2006. Zircon U–Pb and Hf isotope constraints on the Mesozoic tectonics and crustal evolution of southern Tibet. Geology 34, 745–748.
Chung, S.L., Chu, M.F., Zhang, Y.Q., Xie, Y.W., Lo, C.H., Lee, T.Y., Lan, C.Y., Li, X.H., Zhang, Q., Wang, Y.Z., 2005. Tibetan tectonic evolution inferred from spatial and temporal variations in post-collisional magmatism. Earth-Science Reviews 68, 173–196.
Copeland, P., Harrison, T.M., Pan, Y., Kidd, W.S.F., Roden, M., Zhang, Y.Q., 1995. Thermal evolution of the Gangdese batholith, southern Tibet: a history of episodic unroofing. Tectonics 14, 223–236.

Coulon, C., Maluski, H., Bollinger, C., Wang, S., 1986. Mesozoic and Cenozoic volcanic rocks from central and southern Tibet: $^{39}Ar/^{40}Ar$ dating, petrological characteristics and geodynamical significance. Earth and Planetary Science Letters 79, 281–302.
Davidson, J.P., Harmon, R.S., Wörner, G., 1993. The source of Central Andean magmas: some considerations. In: Harmon, R.S. and Rapela, C.W., (eds.), Andean Magmatism and its tectonic setting. Geological Society of America Special Paper 265, 233–243.
Davies, J.H., von Blanckenburg, F., 1995. Slab breakoff: a model of lithospheric detachment and its test in the magmatism and deformation of collisional orogens. Earth and Planetary Science Letters 129, 85–102.
DeCelles, P.G., Kapp, P., Ding, L., Gehrels, G.E., 2007. Late Cretaceous to middle Tertiary basin evolution in the central Tibetan plateau: changing environments in response to tectonic partitioning, aridification, and regional elevation gain. Geological Society of America Bulletin 119, 654–680.
DePaolo, D.J., Weaver, K.L., Mo, X.X., Zhao, Z.D., Harrison, T.M., 2008. Regional isotopic patterns in granitic rocks of southern Tibet and evolution of crustal structure during the Indo-Asian collision. Goldschmidt Conference Abstracts, vol. A211.
Dewey, J.F., Shackleton, R.M., Chang, C.F., Sun, Y.Y., 1988. The tectonic evolution of the Tibetan plateau. Philosophical transactions of the Royal Society of London (Series A): mathematical and physical. Sciences 327, 379–413.
Gao, S., Liu, X.M., Yuan, H.L., Hattendorf, B., Gunther, D., Chen, L., Hu, S.H., 2002. Determination of forty-two major and trace elements in USGS and NIST SRM glasses by laser ablation-inductively coupled plasma-mass spectrometry. Geostandards Newsletter — Journal of Geostandards and Geoanalysis 26, 191–196.
Griffin, W.L., Wang, X., Jackson, S.E., Pearson, N.J., O'Reilly, S.Y., Xu, X., Zhou, X., 2002. Zircon chemistry and magma mixing, SE China: in-situ analysis of Hf isotopes, Tonglu and Pingtan igneous complexes. Lithos 61, 237–269.
Gutscher, M.A., Maury, R., Eissen, J.P., Bourdon, E., 2000. Can slab melting be caused by flat subduction? Geology 28, 535–538.
Guynn, J.H., Kapp, P., Pullen, A., Gehrels, G., Heizler, M., Ding, L., 2006. Tibetan basement rocks near Amdo reveal "missing" Mesozoic tectonism along the Bangong suture, central Tibet. Geology 34, 505–508.
Harris, N.B.W., Xu, R.H., Lewis, C.L., Hawkesworth, C.J., Zhang, Y.Q., 1988a. Isotope geochemistry of the 1985 Tibet Geotraverse: Lhasa to Golmud. Philosophical transactions of the Royal Society of London. Series A, mathematical and physical. Sciences 327 (1594), 263–285.
Harris, N.B.W., Xu, R.H., Lewis, C.L., Jin, C.W., 1988b. Plutonic rocks of the 1985 Tibet Geotraverse, Lhasa to Golmud. Philosophical transactions of the Royal Society of London. Series A, mathematical and physical. Sciences 327 (1594), 145–168.
Harris, N.B.W., Inger, S., Xu, R., 1990. Cretaceous plutonism in Central Tibet: an example of post-collision magmatism? Journal of Volcanology and Geothermal Research 44, 21–32.
He, S.D., Kapp, P., DeCelles, P.G., Gehrels, G.E., Heizler, M., 2007. Cretaceous–Tertiary geology of the Gangdese Arc in the Linzhou area, southern Tibet. Tectonophysics 433, 15–37.
Hoskin, P.W.O., Schaltegger, U., 2003. In: Manchar, J.M., Hoskin, P.W.O. (Eds.), the composition of zircon and igneous and metamorphic petrogenesis. Zircon Reviews of Mineralogy and Geochemistry 53, 27–62.
Hu, D.G., Wu, Z.H., Jiang, W., Shi, Y.R., Ye, P.S., Liu, Q.S., 2005. SHRIMP zircon U-Pb age and Nd isotopic study on the Nyainqêntanglha Group in Tibet. Science in China (Series D) 48, 1377–1386.
Jackson, S.E., Pearson, N.J., Griffin, W.L., Belousova, E.A., 2004. The application of laser ablation-inductively coupled plasma-mass spectrometry to in situ U–Pb zircon geochronology. Chemical Geology 211, 47–69.
Ji, Z.S., Yao, J.X., Wu, G.C., 2007. Stratigraphic division of the marine Triassic in the Coqen area, western Gangdese, Tibet. China. Geological Bulletin of China 26, 947–952 (in Chinese with English abstract).
Ji, W.Q., Wu, F.Y., Chung, S.L., Li, J.X., Liu, C.Z., 2009a. Zircon U–Pb chronology and Hf isotopic constraints on the petrogenesis of Gangdese batholiths, southern Tibet. Chemical Geology 262, 229–245.
Ji, W.Q., Wu, F.Y., Chung, S.L., Liu, C.Z., 2009b. Geochronology and petrogenesis of granitic rocks in Gangdese batholith, southern Tibet. Science in China (series D-Earth Science) 52. doi:10.1007/s11430-009-0131-y.
Kang, Z.Q., Xu, J.F., Dong, Y.H., Wang, B.D., 2008. Cretaceous volcanic rocks of Zenong Group in north-middle Lhasa block: products of southward subducting of the Slainajap Ocean? Acta Petrologica Sinica 24, 303–314 (in Chinese with English abstract).
Kang, Z.Q., Xu, J.F., Wang, B.D., Dong, Y.H., Wang, S.Q., Chen, J.L., 2009. Geochemistry of Cretaceous volcanic rocks of Duoni Formation in northern Lhasa block: discussion of tectonic setting. Earth Science — Journal of China University of Geosciences 34, 89–104 (in Chinese with English abstract).
Kapp, P., Murphy, M.A., Yin, A., Harrison, T.M., Ding, L., Guo, J.R., 2003. Mesozoic and Cenozoic tectonic evolution of the Shiquanhe area of western Tibet. Tectonics 22, 1029. doi:10.1029/2001TC001332.
Kapp, P., Yin, A., Harrison, T.M., Ding, L., 2005a. Cretaceous–Tertiary shortening, basin development, and volcanism in central Tibet. Geological Society of America Bulletin 117, 865–878.
Kapp, J.L.D., Harrison, T.M., Kapp, P., Grove, M., Lovera, O.M., Lin, D., 2005b. Nyainqêntanglha Shan: a window into the tectonic, thermal, and geochemical evolution of the Lhasa block, southern Tibet. Journal of Geophysical Research 110, B08413. doi:10.1029/2004JB003330.
Kapp, P., DeCelles, P.G., Gehrels, G.E., Heizler, M., Ding, L., 2007. Geological records of the Lhasa–Qiangtang and Indo-Asian collisions in the Nima area of central Tibet. GSA Bulletin 119, 917–932.
Keto, L.S., Jacobsen, S.B., 1987. Nd and Sr isotopic variations of Early Paleozoic oceans. Earth and Planetary Science Letters 84, 27–41.
Lee, H.Y., Chung, S.L., Lo, C.H., Ji, J., Lee, T.Y., Qian, Q., Zhang, Q., 2009. Eocene Neotethyan slab breakoff in southern Tibet inferred from the Linzizong volcanic record. Tectonophysics. doi:10.1016/j.tecto.2009.02.031.
Leeder, M.R., Smith, A.B., Yin, J.X., 1988. Sedimentology, palaeoecology and palaeoenvironmental evolution of the 1985 Lhasa to Golmud Geotraverse. Philosophical Transactions of the Royal Society of London, Series A, Mathematical and Physical Sciences 327, 107–143.
Leier, A.L., Decelles, P.G., Kapp, P., Gehrels, G.E., 2007a. Lower Cretaceous strata in the Lhasa Terrane, Tibet, with implications for understanding the early tectonic history of the Tibetan Plateau. Journal of Sedimentary Research 77, 809–825.
Leier, A.L., Kapp, P., Gehrels, G.E., DeCelles, P.G., 2007b. Detrital zircon geochronology of Carboniferous–Cretaceous strata in the Lhasa Terrane, Southern Tibet. Basin Research 19, 361–378.
Liu, D.Z., Tao, X.F., Ma, R.Z., Shi, H., Zhu, L.D., Hu, X. W., 2003. 1: 250, 000 geological report of Coqen County with geological map. Chengdu University of Technology, Chengdu, 163–183 (unpublished, in Chinese).
Liu, Y.S., Gao, S., Yuan, H.L., Zhou, L., Liu, X.M., Wang, X.C., Hu, Z.C., Wang, L.S., 2004. U–Pb zircon ages and Nd, Sr, and Pb isotopes of lower crustal xenoliths from North China Craton: insights on evolution of lower continental crust. Chemical Geology 211, 87–109.
Liu, D.Y., Jian, P., Kröner, A., Xu, S.T., 2006. Dating of prograde metamorphic events deciphered from episodic zircon growth in rocks of the Dabie–Sulu UHP complex, China. Earth and Planetary Science Letters 250, 650–666.
Ludwig, K.R., 2003. Isoplot v. 3.0: a geochronological toolkit for Microsoft Excel. Berkeley Geochronology Center. Special Publication No 4, 1–70.
Macera, P.M., Gasperini, D., Ranalli, G., Mahatsent, R., 2008. Slab detachment and mantle plume upwelling in subduction zones: an example from the Italian South-Eastern Alps. Journal of Geodynamics 45, 32–48.
Maluski, H., Proust, F., Xiao, X.C., 1982. $^{39}Ar/^{40}Ar$ dating of the trans-Himalayan calc-alkaline magmatism of southern Tibet. Nature 298, 152–154.
Mo, X.X., Zhao, Z.D., Deng, J.F., Dong, G.C., Zhou, S., Guo, T.Y., Zhang, S.Q., Wang, L.L., 2003. Response of volcanism to the India–Asia collision. Earth Sciences Frontiers (China University of Geosciences, Beijing), vol. 10, pp. 135–148. in Chinese with English abstract.
Mo, X.X., Dong, G.C., Zhao, Z.D., Zhou, S., Wang, L.L., Qiu, R.Z., Zhang, F.Q., 2005. Spatial and temporal distribution and characteristics of granitoids in the Gangdese. Tibet and implication for crustal growth and evolution. Geological Journal of China Universities 11, 281–290 (in Chinese with English abstract).
Mo, X.X., Hou, Z.Q., Niu, Y.L., Dong, G.C., Qu, X.M., Zhao, Z.D., Yang, Z.M., 2007. Mantle contributions to crustal thickening during continental collision: evidence from Cenozoic igneous rocks in southern Tibet. Lithos 96, 225–242.
Mo, X.X., Niu, Y.L., Dong, G.C., Zhao, Z.D., Hou, Z.Q., Zhou, S., Ke, S., 2008. Contribution of syncollisional felsic magmatism to continental crust growth: a case study of the Paleogene Linzizong volcanic succession in southern Tibet. Chemical Geology 250, 49–68.
Pan, G.T., Ding, J., 2004. Geological map (1:1500000) of Qinghai–Xizang (Tibetan) Plateau and adjacent areas. Chengdu Cartographic Publishing House, Chengdu.
Pan, G.T., Mo, X.X., Hou, Z.Q., Zhu, D.C., Wang, L.Q., Li, G.M., Zhao, Z.D., Geng, Q.R., Liao, Z.L., 2006. Spatial–temporal framework of the Gangdese Orogenic Belt and its evolution. Acta Petrologica Sinica 22, 521–533 (in Chinese with English abstract).
Pearce, J.A., Mei, H.J., 1988. Volcanic rocks of the 1985 Tibet Geotraverse: Lhasa to Golmud. Philosophical Transactions of the Royal Society of London, Series A, Mathematical and Physical Sciences 327, 169–201.
Qiu, R.Z., Zhou, S., Deng, J.F., Li, J.F., Xiao, Q.H., Cai, Z.Y., 2004. Dating of gabbro in the Shemalagou ophiolite in the western segment of the Bangong Co–Nujiang ophiolite belt, Tibet—with a discussion of the age of the Bangong Co–Nujiang ophiolite belt. Geology in China 31, 262–268 (in Chinese with English abstract).
Qu, Y.G., Zhang, S.Q., Zheng, C.Z., Wang, Y.S., Lu, P., Wang, H.S., Li, X.B., Li, Q.W., 2003. The Late Jurassic–Early Cretaceous Rila Formation, Rila Formation Suor clastic rocks and characteristics of biotas in the Yunzhug ophiolite belt, northern Tibet. Geological Bulletin of China 22, 959–963 (in Chinese).
Ramos, V.A., 1999. Plate tectonic setting of the Andean Cordillera. Episodes 22, 183–190.
Royden, L.H., 1993. The tectonic expression of slab pull of continental convergent boundaries. Tectonics 12, 303–325.
Rudnick, R.L., Gao, S., Ling, W.L., Liu, Y.S., McDonough, W.F., 2004. Petrology and geochemistry of spinel peridotite xenoliths from Hannuoba and Qixia, North China craton. Lithos 77, 609–637.
Schwab, M., Ratschbacher, L., Siebel, W., McWilliams, M., Minaev, V., Lutkov, V., Chen, F., Stanek, K., Nelson, B., Frisch, W., Wooden, J.L., 2004. Assembly of the Pamirs: age and origin of magmatic belts from southern Tien Shan to the southern Pamirs and their relation to Tibet. Tectonics 23, TC4002.
Sengör, A.M.C., 1979. Mid-Mesozoic closure of Permo - Triassic Tethys and its implications. Nature 279, 590–593.
Shi, R.D., 2007. Age of Bangong Lake SSZ ophiolite constraints the time of the Bangong Lake–Nujiang Neo-Tethys. Chinese Science Bulletin 52, 936–941.
Sylvester, P.J., 1998. Postcollisional strongly peraluminous granites. Lithos 45, 29–44.
Treloar, P.J., Petterson, M.G., Jan, M.Q., Sullivan, M.A., 1996. A re-evaluation of the stratigraphy and evolution of the Kohistan Arc sequence, Pakistan Himalaya: implications for magmatic and tectonic arc-building processes. Journal of the Geological Society of London 153, 681–693.
Turner, S.P., Platt, J.P., George, R.M.M., Kelley, S.P., Pearson, D.G., Novew, G.M., 1999. Magmatism associated with orogenic collapse of the Betic-Alboran domain, SE Spain. Journal of Petrology 40, 1011–1036.
Volkmer, J.E., Kapp, P., Guynn, J.H., Lai, Q., 2007. Cretaceous–Tertiary structural evolution of the north central Lhasa Terrane, Tibet. Tectonics 26, TC6007. doi: 6010.1029/2005TC001832.
von Blanckenburg, F., Davis, J.H., 1995. Slab breakoff: a model for syncollisional magmatism and tectonics in the Alps. Tectonics 14, 120–131.
Wen, D.R., Liu, D.Y., Chung, S.L., Chu, M.F., Ji, J.Q., Zhang, Q., Song, B., Lee, T.Y., Yeh, M.W., Lo, C.H., 2008. Zircon SHRIMP U–Pb ages of the Gangdese Batholith and implications for Neotethyan subduction in southern Tibet. Chemical Geology 252, 191–201.

Wong, A., Ton, S.Y.M., Wortel, M.J.R., 1997. Slab detachment in continental collision zones: an analysis of controlling parameters. Geophysical Research Letters 24, 2095–2098.
Wu, F.Y., Yang, Y.H., Xie, L.W., Yang, J.H., Xu, P., 2006. Hf isotopic compositions of the standard zircons and baddeleyites used in U–Pb geochronology. Chemical Geology 234, 105–126.
XBGMR (Xizang Bureau of Geology and Mineral Resources), 1991. The Regional Geology of Xikazi and Yadong (Geology Part) Scale 1: 200000 (in Chinese). Geological Publishing House, Beijing, pp. 22–148.
Xu, R.H., Schärer, U., Allègre, C.J., 1985. Magmatism and metamorphism in the Lhasa block (Tibet): a geochronological study. Journal of Geology 93, 41–57.
Yang, J.H., Wu, F.Y., Wilde, S.A., Xie, L.W., Yang, Y.H., Liu, X.M., 2007. Tracing magma mixing in granite genesis: in situ U–Pb dating and Hf-isotope analysis of zircons. Contributions to Mineralogy and Petrology 153, 177–190.
Yang, J.S., Xu, Z.Q., Li, Z.L., Xu, X.Z., Li, T.F., Ren, Y.F., Li, H.Q., Chen, S.Y., Robinson, P.T., 2009. Discovery of an eclogite belt in the Lhasa block, Tibet: a new border for Paleo-Tethys? Journal of Asian Earth Sciences 34, 76–89.
Ye, P.S., Wu, Z.H., Hu, D.G., Jiang, W., Yang, X.D., 2005. Geochemical characteristics of ophiolites in Yongzhu-Guomangcuo. Tibet and its tectonic significance. Geoscience 19, 508–514 (in Chinese with English abstract).
Yin, A., Harrison, T.M., 2000. Geologic evolution of the Himalayan–Tibetan orogen. Annual Review of Earth and Planetary Sciences 28, 211–280.
Yin, J.X., Xu, J.T., Liu, C.J., Li, H., 1988. The Tibetan Plateau: regional stratigraphic context and previous work. Philosophical Transactions of the Royal Society of London, Series A, Mathematical and Physical Sciences 327, 5–52.
Zhang, K.J., Xia, B.D., Wang, G.M., Li, Y.T., Ye, H.F., 2004. Early Cretaceous stratigraphy, depositional environments, sandstone provenance, and tectonic setting of central Tibet, western China. Geological Society of America Bulletin 116, 1202–1222.
Zhang, H.F., Parrish, R., Zhang, L., Xu, W.C., Yuan, H.L., Gao, S., Crowley, Q.G., 2007a. A-type granite and adakitic magmatism association in Songpan–Garze fold belt, eastern Tibetan Plateau: implication for lithospheric delamination. Lithos 97, 323–335.
Zhang, K.J., Zhang, Y.X., Li, B., Zhong, L.F., 2007b. Nd isotopes of siliciclastic rocks from Tibet, western China: constraints on provenance and pre-Cenozoic tectonic evolution. Earth and Planetary Science Letters 256, 604–616.
Zhao, Z.D., Mo, X.X., Niu, Y.L., Zhu, D.C., Dong, G.C., Zhou, S., Yang, Y.H., in press. U–Pb zircon age, geochemical and Sr–Nd–Pb–Hf isotopic constraints on the origin of the Early Cretaceous magmatism from Xainza of Lhasa Terrane, southern Tibet.
Zhou, C.Y., Zhu, D.C., Zhao, Z.D., Xu, J.F., Wang, L.Q., Chen, H.H., Xie, L.W., Dong, G.C., Zhou, S., 2008. Petrogenesis of Daxiong pluton in western Gangdese. Tibet: Zircon U-Pb dating and Hf isotopic constraints: Acta Petrologica Sinica, 24, pp. 348–358 (in Chinese with English abstract).
Zhu, D.C., Pan, G.T., Mo, X.X., Wang, L.Q., Liao, Z.L., Zhao, Z.D., Dong, G.C., Zhou, C.Y., 2006. Late Jurassic–Early Cretaceous geodynamic setting in middle-northern Gangdese: new insights from volcanic rocks. Acta Petrologica Sinica 22, 534–546 (in Chinese with English abstract).
Zhu, D.C., Pan, G.T., Chun, S.L., Liao, Z.L., Wang, L.Q., Li, G.M., 2008a. SHRIMP zircon age and geochemical constraints on the origin of Early Jurassic volcanic rocks from the Yeba Formation, southern Gangdese in south Tibet. International Geology Review 50, 442–471.
Zhu, D.C., Pan, G.T., Wang, L.Q., Mo, X.X., Zhao, Z.D., Zhou, C.Y., Liao, Z.L., Dong, G.C., Yuan, S.H., 2008b. Tempo-spatial variations of Mesozoic magmatic rocks in the Gangdese belt, Tibet, China, with a discussion of geodynamic setting-related issues. Geological Bulletin of China 27, 1535–1550 (in Chinese with English abstract).
Zhu, D.C., Mo, X.X., Zhao, Z.D., Xu, J.F., Sun, C.G., Zhou, C.Y., Wang, L.Q., Chen, H.H., Dong, G.C., Zhou, S., 2008c. Zircon U–Pb geochronology of Zenong Group volcanic rocks in Coqen area of the Gangdese. Tibet and tectonic significance. Acta Petrologica Sinica 24, 401–412 (in Chinese with English abstract).
Zhu, D.C., Pan, G.T., Zhao, Z.D., Lee, H.Y., Kang, Z.Q., Liao, Z.L., Wang, L.Q., Li, G.M., Dong, G.C., Liu, B., 2009a. Early Cretaceous subduction-related adakite-like rocks in the Gangdese, south Tibet: products of slab melting and subsequent melt–peridotite interaction? Journal of Asian Earth Sciences 34, 298–309.
Zhu, D.C., Mo, X.X., Niu, Y.L., Zhao, Z.D., Yang, Y.H., Wang, L.Q., 2009b. Zircon U–Pb dating and in-situ Hf isotopic analysis of Permian peraluminous granite in the Lhasa terrane, southern Tibet: implications for Permian collisional orogeny and paleogeography. Tectonophysics 469, 48–60.
Zhu, D.C., Mo, X.X., Niu, Y.L., Zhao, Z.D., Chung, S.L., Wang, L.Q., Hou, Z.Q., DePaolo, D.J., in press. Whole-rock geochemical and Sr–Nd–Pb isotopic constraints on the origin of the Early Cretaceous magmatism in the central Lhasa Terrane, southern Tibet.
Zhu, D.C., Mo, X.X., Niu, Y.L., Zhao, Z.D., Chung, S.L., Wu, F.Y., Wang, L.Q., Hou, Z.Q., DePaolo, D.J., submitted for publication. The lithospheric architecture of the Lhasa Terrane: Revelation and geodynamic significance.